Space Sci Rev
DOI 10.1007/s11214-016-0285-9

Challenges Handling Magnetospheric and Ionospheric Signals in Internal Geomagnetic Field Modelling

C.C. Finlay[1] · V. Lesur[2] · E. Thébault[3] · F. Vervelidou[4] · A. Morschhauser[4] · R. Shore[5]

Received: 15 March 2016 / Accepted: 29 August 2016

Abstract Measurements of the Earth's magnetic field collected by low-Earth-orbit satellites such as *Swarm* and CHAMP, as well as at ground observatories, are dominated by sources in the Earth's interior. However these measurements also contain significant contributions from more rapidly-varying current systems in the ionosphere and magnetosphere. In order to fully exploit magnetic data to probe the physical properties and dynamics of the Earth's interior, field models with suitable treatments of external sources, and their associated induced signals, are essential. Here we review the methods presently used to construct models of the internal field, focusing on techniques to handle magnetospheric and ionospheric signals. Shortcomings of these techniques often limit the quality, as well as spatial and temporal resolution, of internal field models. We document difficulties in using track-by-track analysis to characterize magnetospheric field fluctuations, differences in internal field models that result from alternative treatments of the quiet-time ionospheric field, and challenges

✉ C.C. Finlay
cfinlay@space.dtu.dk

V. Lesur
lesur@ipgp.fr

E. Thébault
erwan.thebault@univ-nantes.fr

F. Vervelidou
foteini.vervelidou@gfz-potsdam.de

A. Morschhauser
achim.morschhauser2@gfz-potsdam.de

R. Shore
robore@bas.ac.uk

1 DTU Space, Technical University of Denmark, Kongens Lyngby, Denmark

2 Institut de Physique du Globe de Paris, Paris, France

3 Laboratoire de Planétologie et Géodynamique de Nantes, Nantes, France

4 GFZ German Research Centre for Geosciences, Potsdam, Germany

5 British Antarctic Survey, Cambridge, UK

Published online: 27 September 2016

associated with rapidly changing, but spatially correlated, magnetic signatures of polar cap current systems. Possible strategies for improving internal field models are discussed, many of which are described in more detail elsewhere in this volume.

Keywords Geomagnetism · Field modelling · Magnetospheric and ionospheric current systems

1 Introduction

Magnetic measurements contain signatures from current sources both internal and external with respect to the Earth's surface, but the communities studying these two aspects interact surprisingly little. The external field community is primarily concerned with event studies during disturbed conditions, while the internal field community seeks to avoid as far as possible external field signatures that they essentially regard as noise.

The internal field consists primarily of contributions from currents in the core, which dominate on large spatial scales at the Earth's surface, and the magnetized lithosphere which dominate at smaller scales. The large-scale internal field is widely used as a source of orientation information in diverse navigational applications, and is also used by scientists studying space physics (where it provides a co-ordinate system for ionospheric currents, see for example Laundal and Richmond (2016) in this volume), exploration geophysicists, and even biologists studying animal migration; there are many thousands of users of geomagnetic reference fields that provide information on the strength and direction of the large-scale internal field (Thébault et al. 2015c). The small-scale internal field is important for tectonic studies (Purucker and Whaler 2007), especially when satellite and airborne data are integrated (Lesur et al. 2016). As an example, Fig. 1 shows the magnetic inclination of the large-scale internal field as captured by the IGRF-12 model (Thébault et al. 2015b), and the radial component of the smaller-scale lithospheric field, estimated using two years of data from the *Swarm* satellite constellation (Olsen et al. 2016). With a wealth of high quality satellite and ground magnetic data now available to construct models of the internal field, the challenge facing internal field modellers is how to improve these models and push them to higher resolution in both space and time.

The purpose of this article is twofold. First, we wish to provide an entry point for scientists working on the external field to the world of internal geomagnetic field modelling, highlighting opportunities for them to apply their existing expertise in another discipline. Second, we wish to review and draw attention to the problems related to external fields faced by developers of internal field models. These challenges are seldom discussed in the literature. If progress is to be made in better estimating the core and lithospheric fields it is essential that the users of internal field models are aware of their limitations, and that those developing the models actively seek new and improved approaches.

In Sect. 2 we briefly summarize the data sources used today to derive internal geomagnetic field models, in particular the typical data selection criteria regarding geomagnetic disturbance activity and the selection of local times. Examples of commonly used internal field models are briefly introduced. In Sect. 3 we give an overview of the mathematical framework for modelling the near-Earth internal field; treatments of the external field in geomagnetic field models are then described in Sect. 3.2. Having described the context, we then move on to outline what we believe are three outstanding challenges in internal field modelling. First, in Sect. 4, we discuss problems posed by along-track correlated errors due to unmodelled

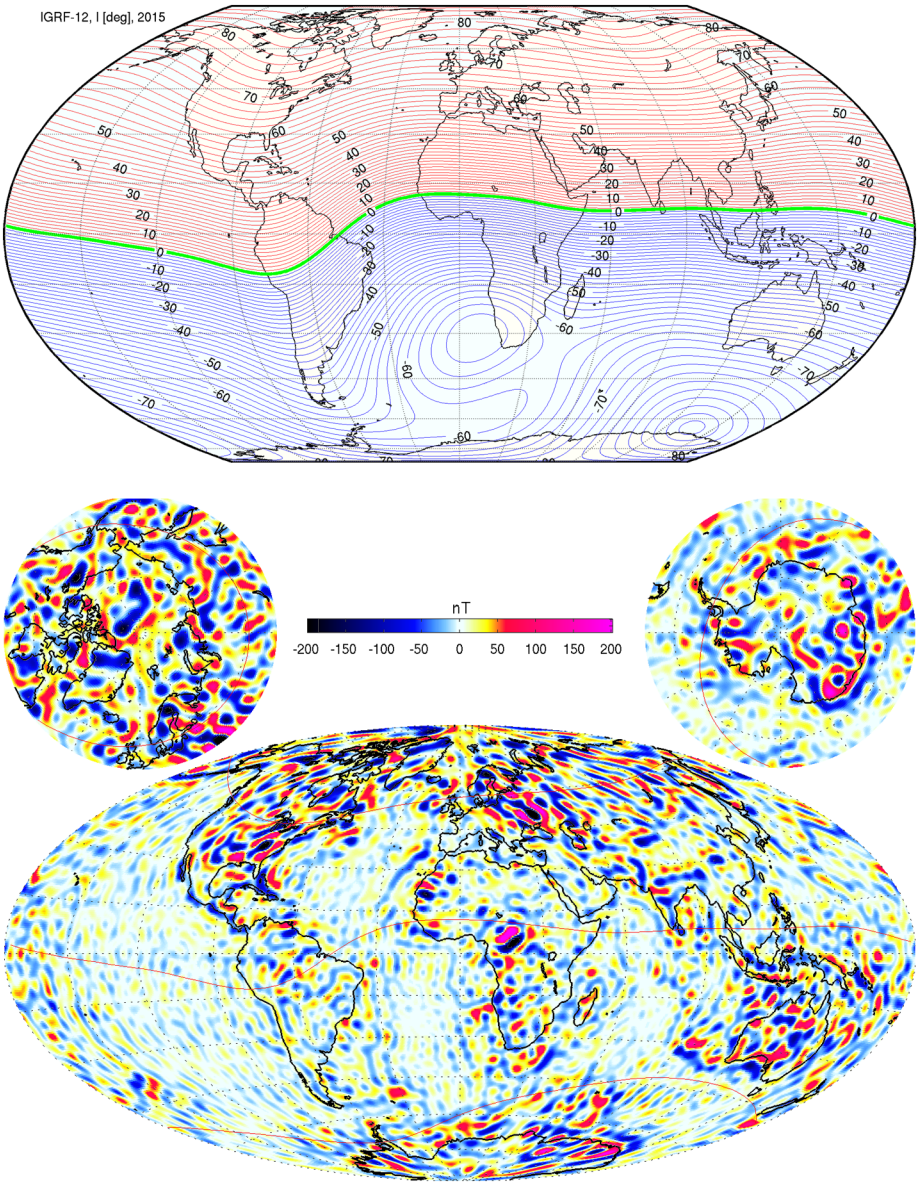

Fig. 1 Examples of internal field models. Top: Magnetic field Inclination at the Earth's surface (units, degrees) as predicted by the IGRF-12 model in epoch 2015.0 (Thébault et al. 2015b). Bottom: Radial magnetic field at the Earth's surface (units, nT) due to lithospheric sources, considering degrees 15–80 from a field model derived from the two years of data from the Swarm satellite constellation (Olsen et al. 2016)

(rapidly-varying) magnetospheric fields, including some undesirable consequences of track-by-track analysis that is often used as a remedy. In Sect. 5 we briefly describe approaches to handling solar quiet ionospheric fields (Sq) and their related induction effects, showing how different modelling treatments can influence estimated internal field. Finally, in Sect. 6 we

describe unmodelled polar current systems and their possible impact on internal field models. We conclude in Sect. 7 with some thoughts concerning avenues for future improvements in internal field modelling.

2 Data Selection for Internal Field Modelling

The first step in constructing models of the internal field typically involves excluding times of enhanced solar-driven external fields, with the remaining *geomagnetically quiet times* usually identified via indices of geomagnetic activity. The review paper by Kauristie et al. (2016) in this volume provides a detailed overview of such geomagnetic indices. Below we summarize the quiet-time criteria employed in some widely used field models; the paramaterization of these models will be discussed in more detail in the following sections.

Quiet time selection criteria are usually based on thresholds for the maximum amplitude or rate of change of geomagnetic indices. Many modellers perform data selection based on the *Dst* index, or similar indices such as the Vector Magnetic Disturbance (*VMD*) index Thomson and Lesur (2007) or the Ring Current (*RC*) index (Olsen et al. 2014), that are designed to track changes in the magnetospheric ring current. This procedure enables periods of enhanced ring current activity to be excluded. Sometimes thresholds are also used for the planetary activity index K_p, which quantifies the range of geomagnetic fluctuations at mid and low latitudes over three hour windows. At high latitudes, additional criteria based on the amplitude and sign of the B_Y and B_Z components of the Interplanetary Magnetic Field (*IMF*) in Geocentric Solar Magnetospheric (*GSM*) coordinates (see e.g. Laundal and Richmond 2016), or quantities derived from the *IMF* but also including information on the solar wind speed (e.g. the merging electric field at the magnetopause, E_m) are used. Some, but not all, modellers carry out additional track-by-track analysis, including rejection of those tracks deemed to show evidence of excessive external disturbance. One notable difference between the selection of data used by different teams is the range of local times considered in the polar regions.

The GRIMM model series is based primarily on CHAMP satellite data (Lesur et al. 2008, 2010; Mandea et al. 2012) and focuses on an accurate estimation of the core and lithospheric fields. Its latest version is described by (Lesur et al. 2015b). It uses three component vector data in the Solar Magnetic (*SM*) coordinate system (see e.g. Laundal and Richmond 2016) for magnetic latitudes below $\pm$ 55 degrees, considering only times when the norm of the VMD index was less than 20 nT and the norm of its time derivative was less than 100 nT per day, when *IMF* B_Z was positive, when the local time was between 23:00 and 05:00 and when the ionosphere was in darkness. At higher magnetic latitudes, three component vector data were used in the North, East, Centre (NEC) coordinate system; data selection at high latitudes was as for low latitudes, except that data from all local times, independent of the sun position, were used.

The CHAOS series of models (Olsen et al. 2006, 2009, 2010, 2014; Olsen and Mandea 2008) is based on satellite data from the Ørsted, SAC-C and CHAMP missions, and most recently also including data from the *Swarm* mission, along with processed ground observatory monthly mean data. The aim is to model the near-Earth, quiet-time, magnetic field to high resolution in space and time. In CHAOS-5 (Finlay et al. 2015), satellite data was used only when the sun was at least 10° below the horizon (i.e. dark times), and when the *RC*-index of magnetospheric ring current activity changed by at most 2 nT/hr; vector data were used at quasi-dipole latitudes below 55 degrees when the activity index

$Kp \leq 2^0$. At higher latitudes, only scalar (intensity) data was used when E_m, defined following Newell et al. (2007) as $0.33 v^{4/3} B_t^{2/3} \sin^{8/3}(|\Theta_{IMF}|/2)$, with v the solar wind speed, and $B_t = \sqrt{B_Y^2 + B_Z^2}$ the magnitude of the *IMF* in the $Y - Z$ plane in GSM coordinates and $\Theta_{IMF} = \arctan(B_Y / B_Z)$, averaged over the preceding one hour, was less than 0.8 mV/m.

The MF series of models (Maus et al. 2002, 2007; Maus 2010) focuses on estimating the lithospheric field to high spherical harmonic degree, using data from the CHAMP mission. The data selection steps used to derive earlier versions of the model are described by Maus et al. (2006b) and Maus et al. (2008). In MF6, scalar and vertical component CHAMP data from local times 22:00 to 05:00, when $Kp \leq 1+$, and at high latitudes when $E_m \leq 0.8$ mV/m were used. Tracks identified as being contaminated by magnetic signals from plasma irregularities in the low-latitude ionosphere, or with abnormally high residuals compared to an internal field reference model were discarded. In MF4, at latitudes above 55 degrees, data were selected only when the magnitude of *IMF* B_Y was less than 8 nT and *IMF* B_Z was between -2 nT and $+6$ nT. In both MF4 and MF6 a large number of tracks were rejected as being disturbed in comparison to neighbouring tracks or through comparisons with reference models. The data processing also involved track-by-track fitting of a model for the polar electrojet.

The Comprehensive Model (CM) series (Sabaka et al. 2002, 2004) takes a different approach, using a broader selection of data and co-estimating a more complete model of the source fields. Internal, ionospheric, and magnetospheric contributions and their induced counterparts are simultaneously co-estimated. In its latest published version, CM5 (Sabaka et al. 2015), magnetic contributions from the ocean tides are also co-estimated. Two levels of data selection were employed in CM5. The first level included data from both disturbed and quiet times, which enabled a description of rapidly varying, aperiodic, fields such as the magnetospheric field and associated induced fields. The second level then focused on estimating the internal fields using data, from geomagnetically quiet times. Vector and scalar data from the Ørsted and CHAMP satellites, and scalar data from the SAC-C mission, as well as observatory hourly mean data were used in CM5. Vector data were used from all local times and at all latitudes, including polar latitudes. For the quiet-time data selection, at non-polar latitudes (equatorward of 60 degrees dipole latitude) only data with $\mathrm{Kp} \leq 2^0$ and for which Dst index does not change by more than 2 nT per hour were used, while for regions poleward of 60 degrees dipole latitude, E_m was required to be below 0.8 mVm^{-1}.

None of the selection criteria described above succeeds in adequately excluding all external fields. A particular problem, discussed in detail elsewhere in this volume (e.g. Kauristie et al. 2016; Friis-Christensen et al. 2016) is finding suitable quiet-time selection criteria in the highly dynamic polar region. We shall briefly return to the issue of data selection in internal field modelling with some comments of our own in Sect. 7.1.

3 Parameterization of Geomagnetic Field Models

3.1 The Internal Field

The most common assumption made in internal field modelling is that the magnetic measurements are made in a source-free region, i.e. where $\nabla \times \boldsymbol{B} = 0$. In this case, the magnetic induction field $\boldsymbol{B}$ (hereafter referred to as the magnetic field) is conservative and it may be represented by a magnetic scalar potential V such that

$$\boldsymbol{B} = -\nabla V. \tag{1}$$

Then, the Laplace equation

$$\nabla^2 V = 0 \tag{2}$$

holds as $\nabla \cdot \boldsymbol{B} = 0$. The solutions to Laplace's equation for V naturally separate into parts due to internal and external sources such that $V = V_{int} + V_{ext}$.

The angular part of the solution to Laplace's equation in spherical geometry may be written in terms of spherical harmonic (SH) functions

$$Y_l^m(\theta, \phi) = \begin{cases} \sin(|m|\phi) P_l^{|m|}(\cos\theta), & \text{if } m < 0 \\ \cos(m\phi) P_l^m(\cos\theta), & \text{if } m \geq 0 \end{cases} \tag{3}$$

where P_l^m are the Schmidt semi-normalized associated Legendre polynomials, l and m are the SH degree and order, respectively, and (θ, ϕ) are spherical geocentric (geographic) coordinates.

Using these spherical harmonics, the scalar magnetic potential V_{int} describing the magnetic field due to internal sources can be expressed as a series expansion of SH functions and

$$V_{int}(r, \theta, \phi) = a \sum_{l=1}^{\infty} \left(\frac{a}{r}\right)^{l+1} \sum_{m=-l}^{l} g_l^m Y_l^m(\theta, \phi) \tag{4}$$

where r is the radius, a is the model's chosen reference radius which is usually set to $a = 6371.2$ km, and g_l^m are the expansion coefficients, also known as the internal Gauss coefficients. In practice, the expansion series is truncated at some degree L which depends on the resolution of the data, and on the target field.

The internal field consists primarily of a time-dependent part generated by dynamo action in the Earth's core and of a quasi-static part due to the magnetization of the lithosphere. In addition, there are smaller contributions due to currents in the mantle that are induced by time-varying external fields, and also fields due to currents in the oceans that are induced as the conducting water moves through the core field. These fields vary on different, but partly overlapping, temporal and spatial scales (e.g. Hulot et al. 2015), making their separation difficult; an example of such a separation problem is discussed in Sect. 5.

Accurate internal field models must take into account the temporal variation of the core field. This is normally achieved by parametrizing the Gauss coefficients g_l^m in time, for example by using a basis of B-spline functions (de Boor 1978; Bloxham and Jackson 1992). Then,

$$g_l^m(t) = \sum_{n=1}^{N} g_{l,n}^m B_{n,k}(t) \tag{5}$$

where $g_{l,n}^m$ are a set of B-spline coefficients for each Gauss coefficient g_l^m. The B-spline basis functions $B_{n,k}$ are piecewise polynomials of order k.

As an example, the $N = 16$ order six B-spline basis functions of the GRIMM-2 model (Lesur et al. 2010) are shown by the dashed lines in Fig. 2. In this case, the functions are defined at knot points with an annual spacing and a $k = 6$ knot multiplicity at the boundaries (2000 and 2011). The resulting time-dependence of g_7^7 (solid black line) is shown along with the respective contributions from the individual splines (coloured lines). The order k of the B-splines defines the smoothness of the time-dependence, and the spacing of the knots limits the temporal resolution. If one wishes to obtain a smooth representation of acceleration of the internal field $\ddot{\boldsymbol{B}}_{int}$, fifth-order or higher B-splines should be used.

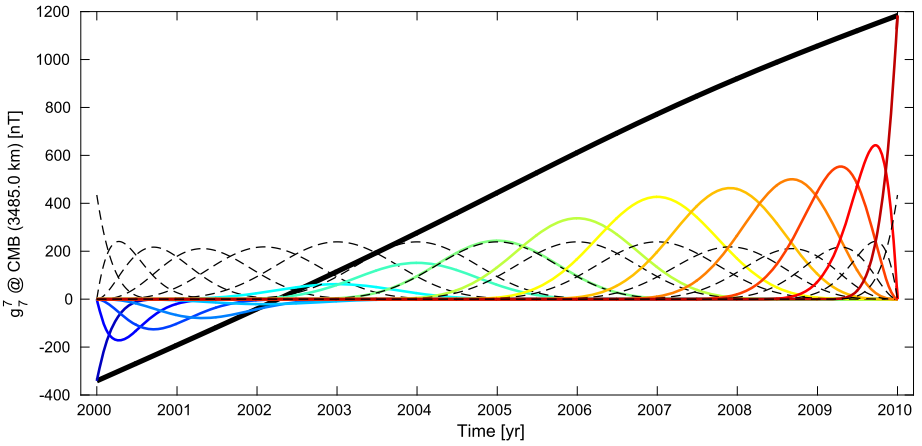

Fig. 2 The time-dependence of the Gauss coefficient for degree $l = 7$ and order $m = 7$ (g_7^7) of the GRIMM-2 model (Lesur et al. 2010) is shown by the *solid black line*. The Gauss coefficients as shown here describe the field at GRIMM-2's reference radius of 3485.0 km, i.e. at the core-mantle boundary. The time-dependence of the GRIMM-2 model is based on order six B-splines with a one year knot spacing. The contributions from each B-spline are shown by the *coloured lines* with the B-spline basis functions shown for reference as *dashed black lines*

Considering short time intervals of up to 2 years, an alternative to using B-splines is to employ a first or second order Taylor expansion around a time of interest (e.g. Chulliat and Maus 2014). In this case, separate models can be derived for chosen time-windows and a way of interpolating the Gauss coefficients between the epochs may be defined.

Perhaps the most widely used internal field model is the International Geomagnetic Reference Field (IGRF) model. It is used, for example, in space physics coordinate systems and ground-based applications, to represent the large-scale field of internal origin. It provides Gauss coefficients at five year intervals between 1900 and 2015, with linear interpolation recommended between these epochs. In addition, it provides an estimate of the expected rate of change of the field for the upcoming five years. The IGRF model is produced by the working group V-MOD of the International Association of Geomagnetism and Aeronomy (IAGA) (Thébault et al. 2015b; Langel 1992) and consists of a weighted average of submitted candidate models from international teams (Thébault et al. 2015a). Each candidate model is extracted from a parent field model that aimed to isolate the internal field signature by modelling or minimizing the contributions from external sources. Another widely used model, also updated every five years, is the World Magnetic Model (WMM) which is jointly derived by the US National Geophysical Data Center (NGDC) and the British Geological Survey (BGS) and which is mainly intended for military and civilian navigation purposes (Chulliat et al. 2015). In addition to these models that are designed primarily for operational purposes, a number of models exist that are designed for high resolution scientific studies of the core and lithospheric fields. These differ most notably in the way the external magnetospheric and ionospheric fields are parameterized, as discussed in detail in the next sections.

The latest version of the CHAOS series of models at the time of preparing this article, CHAOS-5 (Finlay et al. 2015), is provided up to degree and order $L = 90$, with coefficients up to $L = 20$ being time-dependent via order six B-splines with a six-month knot separation. The chosen reference radius in this case is the standard choice of the Earth's reference spherical radius $a = 6371.2$ km. The temporal complexity of the model is controlled by

minimizing norms of the third time derivative throughout the model timespan and the second time derivative at the model endpoints, both evaluated at the core-mantle boundary.

The latest version of the GRIMM model series (Lesur et al. 2015b), is expanded up to degree and order $L = 30$. Coefficients up to $L = 18$ were parametrized in time with order six B-splines with half yearly knot intervals. This model is also regularized in time by minimizing the third time derivative throughout the model as well as the second derivative at the model endpoints. The lithospheric field contribution is handled independently up to SH degree 110 (Lesur et al. 2013). Recent derivatives of the GRIMM model series have been prepared as a Level-2 product of the *Swarm* mission (Rother et al. 2013) and as a candidate for IGRF-12 (Lesur et al. 2015a). In both the CHAOS and GRIMM model series the internal and large-scale external magnetospheric fields are co-estimated (see next section).

In the POMME series of models (Maus et al. 2005, 2006, 2010), prior to the model construction, predictions of various field components are subtracted from the data a priori, including the field induced in oceans (Kuvshinov and Olsen 2005), and a magnetospheric field model (Lühr and Maus 2010). The time-dependence of the POMME model coefficients involves a piece-wise Taylor expansion up to order two (Maus et al. 2010). The POMME series is also used during the construction of the MF series of lithospheric field models. The most recent version, MF7, is parameterized up to SH degree 133.

The internal part of the latest Comprehensive Model, CM5 (Sabaka et al. 2015), is expanded up to degree and order 120, with time-dependence implemented up to degree and order 20 with cubic B-splines at 0.5 yr knot intervals. A version using *Swarm* data is now available as a *Swarm* Level-2 data product (Olsen et al. 2013; Sabaka et al. 2013).

An important aspect of field models built using satellite vector field data is their need for Euler angles (or Quaternions) that describe the rotations of the measured vector components from the 3-axis magnetometer system into the Earth-centered-Earth-Fixed system that is relevant to geomagnetic field models (e.g. Olsen et al. 2006). In some modern field models the crucial Euler angles (or the equivalent Quaternion) for the rotation between the star camera coordinate system and the vector magnetometer coordinate system are co-estimated during the derivation of the field model (Olsen et al. 2006; Maus et al. 2006; Rother et al. 2013; Sabaka et al. 2015). As was pointed out by Olsen et al. (2004), unmodelled toroidal magnetic fields (for example resulting from field aligned currents) can map into effective variations of the Euler angles (or the equivalent Quaternion) designed to account for small variations in the star camera alignments. A recent study by Maus (2015) has highlighted a distinctive local-time dependence of Euler angles co-estimated from CHAMP and *Swarm* data. It seems plausible that these may be reflection of a local-time dependence of unmodelled external field variations, although other explanations are possible. A number of studies are now underway to clarify this issue.

In our opinion, the factor that limits the accuracy of today's internal field models is not an incomplete parameterization of the core and lithospheric fields. Rather it is the incomplete treatment (and difficulty in separating) magnetospheric and ionospheric fields, and their associated induced fields. In the remaining sections we describe how these effects are presently treated in geomagnetic field models, highlighting some problems and shortcomings with the existing techniques.

3.2 The Near-Earth Magnetospheric Field and Related EM Induction

Early models of the large-scale, quiet-time, near-Earth magnetospheric field pre-dated the launch of the Magsat satellite in 1979, but they failed to describe accurately, either in direction or in strength, this contribution at ground observatory or satellite positions (Langel

1987). The first reasonable model of the large-scale magnetospheric field was presented by Langel et al. (1980) using vector field data collected by Magsat. This model was based on a degree one SH representation of the external magnetic scalar potential. No time-dependence was used, so it gave only information on the absolute baseline of the *Dst* index (Sugiura and Kamei 1991). The determination of the *Dst* baseline was, and remains, one of the major difficulties in modelling the external magnetospheric field. Soon after, in 1985, Langel and Estes proposed further magnetospheric field models, still using only the first SH degree, but incorporating a scaling of the *Dst* index to parameterise the temporal variations of this field (Langel and Estes 1985b). The field induced in the conductive layers of the Earth by variations of this external field was also modelled through a simple scaling of the *Dst*.

Using Magsat data from either dawn or dusk, or from a selection of POGO data, Langel and Estes (1985b) were able to study a possible local time dependence in the *Dst* baseline, and to investigate the evolution of the latter between the POGO era and the Magsat eras. The Langel and Estes (1985b) magnetospheric model was also used in the construction of a very influential model of the internal geomagnetic main field for 1980 (Langel and Estes 1985a). Most recent models of the near-Earth magnetospheric field still rely on a very similar parameterisation. The parameterization of the external field introduced by Langel and Estes (1985b) involves expanding the external magnetic potential in SH (recall Eq. (4)) as follows:

$$V_{ext}(r,\theta,\phi,t) = a\sum_{l=1}^{L}\left(\frac{r}{a}\right)^{l}\sum_{m=-l}^{l} q_l^m(t)Y_l^m(\theta,\phi). \tag{6}$$

The maximum SH degree is $L = 1$ and the time dependence for the three external coefficients takes the form: $q = \widetilde{a} + \widetilde{b}\,Dst$ where $\widetilde{a}$ and $\widetilde{b}$ are constant scale factors. The fields induced in the conductive layers of the Earth are assumed to be directly proportional to the inducing field and aligned with the rotation axis of the Earth—i.e. $g_1^0 = \alpha\, q_1^0$, the contributions of the other terms g_1^1 and g_1^{-1} are neglected. A value of $\alpha = 0.27$ was employed.

No further advances in the magnetospheric part of field models were made until a daily and seasonal variation of the *Dst* baseline and scaling was introduced into *GSFC* models by Sabaka and Baldwin (1993). Considering a longer time-span Langel et al. (1996) and then Sabaka et al. (1997) used a model based on B-splines for the time-dependence of a SH degree one external field model. The time variations of this external field model were partly controlled by yearly averages of the *aa* index (for a description of the *aa* index, see the article in this volume by Kauristie et al. (2016)). A higher truncation degree of the spherical harmonic expansion was also used in some cases (see for example in Quinn et al. 1997).

With the launch of the Ørsted satellite in 1999 and the CHAMP satellite in 2000, a series of models that routinely used a SH representation of the large scale external field were developed as candidates for the IGRF (e.g. Olsen et al. 2000; Macmillan and Quinn 2000). Given the shortness of the satellite data series at this time, the temporal parameterisation of the magnetospheric field remained simple. Typically, it involved a constant baseline and a scaling term for *Dst* with induced fields parameterised as being linearly dependent on *Dst*, as in Langel and Estes (1985a)—see Eq. (6).

As a successor to the *GSFC* series of models, T. Sabaka and co-authors introduced in 2000 the Comprehensive Model (CM—Sabaka et al. 2000, 2002) that included a series of innovations. The magnetospheric fields were estimated up to SH degree 8, in a dipolar system of coordinates. Their time dependence, as in Sabaka and Baldwin (1993), included a scaling of *Dst*, but also daily and seasonal variations. The induced fields were, as before, dependent on *Dst*, but the scaling was different for each harmonic degree in order to account for a 1-D distribution of the Earth's conductivity. The exact parameterisation of the CM

magnetospheric field and of its induced counterpart is too complex to be reported in detail here. Interested readers should refer to the original paper: Sabaka et al. (2002).

The increasing complexity of the temporal parameterisation of the *Dst* index baseline triggered the development of models not depending on *Dst*. In Lesur et al. (2005) daily values of the three internal and external SH degree one Gauss coefficients were estimated. This revealed a clear external field signal correlated with the variation of the *IMF*, in particular its B_Y component. Its origin has been attributed to field aligned currents by Vennerstrom et al. (2007).

Computing daily values without temporal smoothness carries the risk, already identified in Cain et al. (1989), that the highest SH degree tesseral Gauss coefficients of lithospheric field models will be erroneous. This difficulty has been studied in detail by Thébault et al. (2012) and Lesur et al. (2013) and is also reviewed in Sect. 4 below. Despite concerns over the estimation of low degree external fields on relatively short time spans, this approach has been used in many recent models (e.g. Olsen et al. 2014; Sabaka et al. 2015). In the latter study, possible cross-talk between magnetospheric and lithospheric Gauss coefficients was examined, and estimated to be a rather small effect.

Combining the accumulated knowledge, Maus and Lühr (2005) proposed a model without time dependence but using a SH representation in SM and GSM coordinates. Rapid variations of the external fields were as before modelled using *Dst*, but also a dependence on *IMF* was introduced. The *Dst* index was decomposed in external and induced parts as proposed by Maus and Weidelt (2004) (see also Olsen et al. 2005). This model was later updated by Lühr and Maus (2010). The idea to define a parameterisation of the external field in GSM and/or SM coordinate systems is now used in the magnetsopheric parts of many other field models.

The original parameterisation of Maus and Lühr (2005) can be summarized by the following summation of spherical harmonic expansions of the potential:

$$V(r,\theta,\phi) = a\sum_{l=1}^{L}\sum_{m=-l}^{l}\left[q_l^m(t)\left(\frac{r}{a}\right)^l + \left(\alpha_l^m(t)+\delta_l^m(t)\right)\left(\frac{a}{r}\right)^{l+1}\right]Y_l^m(\theta,\phi), \tag{7}$$

where the three coefficients q_l^m, α_l^m, δ_l^m correspond to one external and two internal (induced) field parameters respectively, in an Earth fixed reference system. They are time-dependent and defined by:

$$\begin{cases} q_l^m(t) = \displaystyle\sum_{m'=-l}^{l}\sum_{k,j=0}^{N} \mathcal{R}e\left\{A_{l,m,m',j}\exp(ij\omega_a t)\right\} \\ \qquad \times \mathcal{R}e\left\{D_{l,m,m',k}\exp(ik\omega_d t)\right\}\tilde{q}_l^{m'} \\ \alpha_l^m(t) = \displaystyle\sum_{j=0}^{N} \mathcal{R}e\left\{q_l(j\omega_a)A_{l,m,m',j}\exp(ij\omega_a t)\right\} \\ \qquad \times \mathcal{R}e\{D_{l,m,m',0}\}\tilde{q}_l^{m'} \\ \delta_l^m(t) = \displaystyle\sum_{m'=-l}^{l}\sum_{k,j=0}^{N} \mathcal{R}e\left\{A_{l,m,m',j}\exp(ij\omega_a t)\right\} \\ \qquad \times \mathcal{R}e\left\{q_l(k\omega_d)D_{l,m,m',k}\exp(ik\omega_d t)\right\}\tilde{q}_l^{m'} \end{cases} \tag{8}$$

where $\mathcal{R}e\{X\}$ is the real part of the complex number X, $\omega_a = 2\pi/a$ are annual frequencies with a the number of second in a year, $\omega_d = 2\pi/d$ are diurnal frequencies with d the number of second in a day. The maximum values for k and j are $N = 3$. The complex

coefficients $A_{l,m,m',j}$ and $D_{l,m,m',k}$ allow the computation of q_l^m from the Gauss coefficient $\tilde{q}_l^{m'}$ in the GSM or SM reference frame. Finally, $q_l(\omega)$ are the values of a transfer function that corresponds to the ratio between induced and inducing fields at a given frequency. This dependence on the frequency is introduced to account for the variation with depth of the Earth's conductivity.

In their application, Maus and Lühr (2005) used only the Gauss coefficients $\tilde{q}_1^{0,\mathrm{SM}}$, $\tilde{q}_2^{1,\mathrm{SM}}$, $\tilde{q}_2^{-1,\mathrm{SM}}$, and all the $\tilde{q}_l^{m,\mathrm{GSM}}$ for $l = 1, 2$. All coefficients were assumed constant in time except for $\tilde{q}_1^{0,\mathrm{SM}}$, $\tilde{q}_1^{1,\mathrm{GSM}}$ and $\tilde{q}_1^{-1,\mathrm{GSM}}$ that were linearly dependent on the *Dst*, *IMF* B_x and *IMF* B_y, respectively. The complexity of the model comes mainly from the attempt to account for the change of the Earth's conductivity with depth. The scheme becomes easy to handle for transfer functions that are independent of frequency.

With the accumulation of satellite data from the CHAMP mission, it was soon recognised that the lack of a proper baseline for the *Dst* index was still a problem. To handle this, together with the delays in the production of the definitive values of the *Dst* index, several new indices were proposed. Thomson and Lesur (2007) introduced the *VMD* index, derived from all available observatory data, that is a 3 component index with a baseline that is stable over 4 months. As a result the parameterisation of the absolute value of the baseline remains simple (e.g. Lesur et al. 2010). The derivation of the *VMD* index has been adapted to satellite data (Kunagu et al. 2013) (the *SVMD* index), and is the underlying idea associated with the derivation of the *MMA* Level-2 product of the Swarm satellite mission (Hamilton 2013). These indices have been used in a number of field models (e.g. Lesur et al. 2015b; Rother et al. 2013). It should be noted that in principle these vector indices absorb signals such as those correlated with the *IMF*.

In the latest model of the GRIMM series (Lesur et al. 2015b), the external and induced counterpart fields are modelled through an external and an induced potential:

$$
\begin{aligned}
V_{ext} = a \sum_{l,m}^{20} \left(\frac{r}{a}\right)^l q_l^m \, Y_l^m(\theta, \phi) \\
+ a \left\{ q_{1j}^{0,\mathrm{GSM}} \, Y_1^0(\theta_{\mathrm{GSM}}, \phi_{\mathrm{GSM}}) \right\} \\
+ a \sum_{j=1}^{N_e} \left\{ q_{1j}^{0,\mathrm{SM}} \, Y_1^0(\theta_{\mathrm{SM}}, \phi_{\mathrm{SM}}) + q_{1j}^{-1\,\mathrm{SM}} \, Y_1^{-1}(\theta_{\mathrm{SM}}, \phi_{\mathrm{SM}}) \right\} \mathcal{H}_j(1) \\
+ a \sum_{j=1}^{N_e} \left\{ \sum_{m=-1}^{1} q_{1j}^{m,\mathrm{SVMD}} \, Y_1^m(\theta_{\mathrm{SM}}, \phi_{\mathrm{SM}}) \right\} \mathcal{H}_j(\mathrm{SVMD}_m) \\
+ a \sum_{j=1}^{N_e} \left\{ \left(\frac{r}{a}\right) q_{2j}^{0,\mathrm{SVMD}} \, Y_2^0(\theta_{\mathrm{SM}}, \phi_{\mathrm{SM}}) \right\} \mathcal{H}_j(\mathrm{SVMD}_0),
\end{aligned}
\tag{9}
$$

and,

$$
V_{int} = a \sum_{j=1}^{N_e} \left\{ \left(\frac{a}{r}\right)^2 g_1^{0,\mathrm{ind}} \, Y_1^0(\theta_{\mathrm{SM}}, \phi_{\mathrm{SM}}) \right\} \mathcal{H}_j(\mathrm{I_{dst}}), \tag{10}
$$

where $\mathcal{H}_j(X)$ takes the value X in the 100-day time interval $[t_j; t_{j+1}]$ and is zero elsewhere. These 100-day time intervals match the time intervals on which the *SVMD* index was built with a constant baseline. The index I_{dst} is the induced internal part of the *Dst* index derived

assuming an Earth conductivity model (Maus and Weidelt 2004; Olsen et al. 2005). The angles $(\theta_{\mathrm{SM}}, \phi_{\mathrm{SM}})$ and $(\theta_{\mathrm{GSM}}, \phi_{\mathrm{GSM}})$ are the co-latitudes and longitudes in *SM* and *GSM* coordinates respectively.

In a parallel effort, Olsen et al. (2014) introduced the *RC* index that is, like the *Dst*, a scalar index following the variations of the ring current. The *RC* index is obtained by hour-by-hour (Huber-weighted) spherical harmonic analysis of a selection of mid and low latitude observatories, after subtraction of an internal field model, and it possesses a more stable baseline than *Dst*. The parameterization of the large-scale magnetospheric field adopted in the CHAOS series of field models (Olsen and Mandea 2008; Olsen et al. 2006, 2009, 2010, 2014; Finlay et al. 2015) is broadly similar. We provide here the parametrization for the latest model:

$$V^{\mathrm{ext}} = a \sum_{l=1}^{2} \sum_{m=-l}^{l} q_l^{m,\mathrm{SM}} \left(\frac{r}{a}\right)^l Y_l^m(\theta_{\mathrm{SM}}, \phi_{\mathrm{SM}}) + a \sum_{l=1}^{2} q_l^{0,\mathrm{GSM}} \left(\frac{r}{a}\right)^l Y_l^0(\theta_{\mathrm{GSM}}, \phi_{\mathrm{GSM}}) \tag{11}$$

The degree-1 coefficients in *SM* coordinates are time-dependent and are further expanded as

$$q_1^{0,\mathrm{SM}}(t) = \hat{q}_1^0 \left[\epsilon(t) + \iota(t)\left(\frac{a}{r}\right)^3\right] + \Delta q_1^0(t) \tag{12a}$$

$$q_1^{1,\mathrm{SM}}(t) = \hat{q}_1^1 \left[\epsilon(t) + \iota(t)\left(\frac{a}{r}\right)^3\right] + \Delta q_1^1(t) \tag{12b}$$

$$q_1^{-1,\mathrm{SM}}(t) = \hat{q}_1^{-1} \left[\epsilon(t) + \iota(t)\left(\frac{a}{r}\right)^3\right] + \Delta q_1^{-1}(t) \tag{12c}$$

where the terms in brackets describe the contributions from the magnetospheric ring-current and its Earth-induced counterpart as estimated by the *RC* index, $RC(t) = \epsilon(t) + \iota(t)$. $\hat{q}_1^0$, $\hat{q}_1^1$, $\hat{q}_1^{-1}$ are time-independent regression factors and Δq_1^0, Δq_1^1 and Δq_1^{-1} are time-varying *RC* baseline corrections estimated, for example, in bins of 5 days (for Δq_1^0) and 30 days (for Δq_1^1, Δq_1^{-1}), respectively. The main difference between the CHAOS and GRIMM formulations comes from the length of the time interval on which the coefficients are estimated. Justifications for the modeller's choices are given in the original papers.

The fundamental principles of how magnetospheric fields are included in geomagnetic field models have not changed over the past 30 years and remain rather simple: external fields are modelled through a spherical harmonic expansion due to external sources that is truncated at relatively low degree. This procedure precludes a physical separation of the different sources external to the measurements that include the ring current, magnetotail currents, field aligned currents and all other possible systems of currents. Our magnetospheric modelling technique has evolved only in how it seeks to handle the time dependence. Nonetheless, no matter how complex the time dependence is made, the models still fail to fit all the detail of the observed variations of external fields. An example is given in Fig. 3 where quiet-time residuals between ground observatory data and a geomagnetic field model show features that are not accounted for by fluctuations of *Dst* or by fluctuations of IMF B_y. As a result, the residual external field signals dominate instrumental errors and can leak inside models of the core and lithosphere.

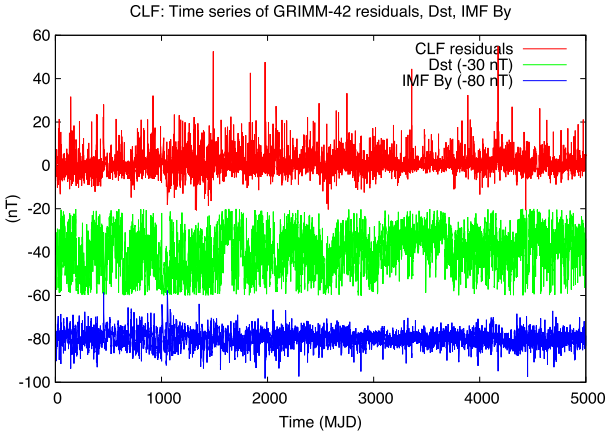

Fig. 3 In red: Time series of Chambon-La-Forêt hourly mean residuals, $X_{SM}(t)$ component, after subtracting the GRIMM42 magnetic model. In green: Dst index time series with 30 nT subtracted. In blue: *IMF* B_Y time series with 80 nT subtracted. The data have been selected for magnetically quiet times. In particular Dst values range between −30 and 10 nT. Large peaks are still visible in the residuals that do not correspond to any specific signals in *Dst* or *IMF*. MDJ = Modified Julian Day 2000

There is a limit to the temporal complexity we can give to the external field models. As will be discussed in the next section, an index baseline—e.g. for the *Dst* baseline, that is estimated for each satellite orbit may affect all components of internal field models. To circumvent this problem it is necessary to use a system of representation of the fields that contains sufficient information on their origin for the internal and external contributions to separate naturally, even with a relatively small number of data points (see also Sect. 7.2). Attempts to use other magnetospheric field models, such as the Tsyganenko model (Tsyganenko 2000, 2002a,b) models, have shown that they do not provide precise enough estimates of the near-Earth magnetic field contributions (Woodfield et al. 2007; Zhang et al. 2010). Comparisons of low-Earth orbit satellite data and ground observatory data with global numerical models of the magnetosphere are rare, and often only single storm events are considered (e.g. Namgaladze et al. 2000).

4 Leakage of the Large-Scale External Field and Track-by-Track Analysis Schemes

Having now introduced common techniques used to parameterize internal and large scale external (magnetospheric) fields in contemporary geomagnetic field models, we now move on to present three examples of outstanding challenges in internal field modelling that are not well dealt with by existing techniques.

In this section, we present in detail a particular approach (track-by-track or along-track analysis) that is commonly adopted in high degree lithospheric field modelling in an attempt to deal with large-scale, but rapidly time-varying, external and related induced fields. The problem in this case is that contributions from temporally-varying, large-scale, external sources can easily be misinterpreted as spatial variations of the static lithospheric field, as the satellite moves from one orbit to the next. This is due to space-time aliasing between the signals. The accuracy with which one removes the effects of disturbance fields (for example related to the magnetospheric ring current) determines the quality of recovery of small scales in lithospheric field models.

A common approach for dealing with large-scale, rapidly-varying, external fields in the context of sequential modelling (see, e.g. Langel et al. 1982; Arkani-Hamed et al. 1994; Neubert et al. 2001; Maus et al. 2006a) consists of considering this field, and its induced

counterpart to be static along a given satellite track, i.e. half-orbit. This assumed geometry allows only zonal signals (i.e. of SH order $m = 0$) to be recovered. The sum of this external field and its induced counterpart, together denoted $\tilde{\mathbf{B}}^0$, involves a SH expansion of the following form:

$$\tilde{B}_r^0 = \sum_{w=1}^{w_{max}} \left\{ (w+1)\tilde{g}_w^0 \left(\frac{a}{r}\right)^{w+2} - w\tilde{q}_w^0 \left(\frac{r}{a}\right)^{w-1} \right\} P_w^0(\cos\theta) \tag{13}$$

$$\tilde{B}_\theta^0 = -\sum_{w=1}^{w_{max}} \left\{ \tilde{g}_w^0 \left(\frac{a}{r}\right)^{w+2} + \tilde{q}_w^0 \left(\frac{r}{a}\right)^{w-1} \right\} \frac{dP_w^0(\cos\theta)}{d\theta} \tag{14}$$

$$\tilde{B}_\phi^0 = 0, \tag{15}$$

where $P_w^0(\theta)$ is the Legendre polynomial of degree w, $\tilde{q}_w^0$ the estimate of the true external Gauss coefficient q_w^0 and $\tilde{g}_w^0$ the estimate of the true internal Gauss coefficient g_w^0. The latter describes the induced counterpart of the magnetospheric signal. The maximum SH degree w_{max} is usually restricted to one or two, but here we keep the formalism as general as possible, following the presentation of Thébault et al. (2012).

In track-by-track analysis, the coefficients $\tilde{q}_w^0$ and $\tilde{g}_w^0$ are estimated separately for each available satellite track through a least-squares (LS) inversion of the data, denoted $\mathbf{B}$. The solution is that minimizing the cost function

$$\chi^2 = \int_0^\pi \left(\mathbf{B} - \tilde{\mathbf{B}}^0\right)^2 \sin\theta d\theta \tag{16}$$

If

$$\iota_n^m(\phi) = g_n^m \cos(m\phi) + h_n^m \sin(m\phi) \tag{17}$$

$$\epsilon_n^m(\phi) = q_n^m \cos(m\phi) + s_n^m \sin(m\phi), \tag{18}$$

where $\{g_n^m, h_n^m\}$ and $\{q_n^m, s_n^m\}$ are the internal, respectively external, Gauss coefficients of degree n and order m of $\mathbf{B}$, and

$$\gamma_{w,n}^m = \frac{\langle P_w^0, P_n^m \rangle}{\| P_w^0 \|} \quad \text{and} \quad \beta_{w,n}^m = \frac{\langle \frac{dP_w^0}{d\theta}, \frac{dP_n^m}{d\theta} \rangle}{\| \frac{dP_w^0}{d\theta} \|}, \tag{19}$$

with

$$\langle f, g \rangle = \int_0^\pi fg \sin\theta d\theta \quad \text{and} \quad \| f \|^2 = \langle f, f \rangle \tag{20}$$

then least-squares estimates for the track-by-track model coefficients take the form (Thébault et al. 2012)

$$\tilde{q}_w^0 = \frac{1}{2w+1} \sum_{n=1}^{\infty} \sum_{m=0}^{n} \Bigg[\beta_{w,n}^m (w+1) \left\{ \iota_n^m(\phi) \left(\frac{a}{r}\right)^{n+w+1} + \epsilon_n^m(\phi) \left(\frac{r}{a}\right)^{n-w} \right\}$$
$$+ \gamma_{w,n}^m \left\{ n\iota_n^m(\phi) \left(\frac{r}{a}\right)^{n-w} - (n+1)\epsilon_n^m(\phi) \left(\frac{a}{r}\right)^{n+w+1} \right\} \Bigg] \tag{21}$$

$$\tilde{g}_w^0 = \frac{1}{2w+1}\sum_{n=1}^{\infty}\sum_{m=0}^{n}\Bigg[\beta_{w,n}^m w\left\{\iota_n^m(\phi)\left(\frac{a}{r}\right)^{n-w} + \epsilon_n^m(\phi)\left(\frac{r}{a}\right)^{n+w+1}\right\}$$
$$+\gamma_{w,n}^m\left\{(n+1)\iota_n^m(\phi)\left(\frac{a}{r}\right)^{n-w} - n\epsilon_n^m(\phi)\left(\frac{r}{a}\right)^{n+w+1}\right\}\Bigg], \tag{22}$$

On the basis of these expressions, Thébault et al. (2012) pointed out several drawbacks of track-by-track analysis. First, it becomes apparent that any internal contributions, including the lithospheric field, that have not been properly accounted for, will leak into the inferred external field model. This produces a spurious variation with respect to longitude in the inferred external field model, violating the initial assumption of a zonal geometry. Moreover, this leakage will cause two tracks at the same longitude but different altitudes to show a false time variation. In addition, the external coefficients $\tilde{q}_w^0$ and the internal coefficients $\tilde{g}_w^0$ are hard to distinguish from each other, leading to difficulties in computing upper mantle conductivities (e.g. Civet et al. 2015; Püthe et al. 2015).

In sequential track-by-track analysis, the field $\tilde{\mathbf{B}}^0$, obtained by putting Eqs. (21) and (22) into Eqs. (13) to (15), is removed from the data before lithospheric field modelling. Of course the aforementioned artefacts affecting the description of $\tilde{\mathbf{B}}^0$ will then propagate into the lithospheric field models.

Thébault et al. (2012) show that part of the artefacts may be avoided if the data obtained after removal of the track-by-track estimated field $\tilde{\mathbf{B}}^0$ is not simply mapped, but inverted in a least-squares sense for a static internal SH expansion of the scalar potential V, of the form

$$V = a\sum_{l=1}^{l_{max}}\sum_{k=0}^{l}\left(\frac{a}{r}\right)^{l+1}\left[\tilde{g}_l^k\cos(k\phi) + \tilde{h}_l^k\sin(k\phi)\right]P_l^k(\cos\theta), \tag{23}$$

where $\{\tilde{g}_l^k, \tilde{h}_l^k\}$ are the estimates of the true lithospheric field coefficients $\{g_l^k, h_l^k\}$.

In this case, the result of a least square inversion for the static internal field may be shown to be (Thébault et al. 2012)

$$\begin{Bmatrix}\tilde{g}_l^k\\ \tilde{h}_l^k\end{Bmatrix} = \begin{Bmatrix}g_l^k\\ h_l^k\end{Bmatrix}$$
$$-\sum_{w=1}^{w_{max}}\sum_{n=1}^{\infty}\begin{Bmatrix}g_n^k\\ h_n^k\end{Bmatrix}\left(\frac{a}{r}\right)^{n-l}\frac{(n+1)(l+1)\gamma_{w,n}^k\gamma_{w,l}^k\|P_w^0\|^2 + \beta_{w,n}^k\beta_{w,l}^k\|\frac{dP_w^0}{d\theta}\|^2}{(2l+1)(l+1)\|P_l^k\|^2}$$
$$-\sum_{w=1}^{w_{max}}\sum_{n=1}^{\infty}\begin{Bmatrix}q_n^k\\ s_n^k\end{Bmatrix}\left(\frac{r}{a}\right)^{l+n+1}\frac{(-n)(l+1)\gamma_{w,n}^k\gamma_{w,l}^k\|P_w^0\|^2 + \beta_{w,n}^k\beta_{w,l}^k\|\frac{dP_w^0}{d\theta}\|^2}{(2l+1)(l+1)\|P_l^k\|^2} \tag{24}$$

This expression further demonstrates the manner in which external field estimation artefacts can leak into the internal field model, contaminating all three field components, despite the fact that $\tilde{B}_\phi^0 = 0$. The estimated coefficients of Eq. (24) involve a sum of the true coefficients and an error term. The error term depends on external and internal contributions at all SH degrees, including the contributions from the lithospheric field itself.

An example of the contamination of the radial magnetic field in a static internal field model that can result from track-by-track analysis, via the error term in Eq. (24), is presented in Fig. 4. This is based on sequential track-by track analysis applied to synthetic data constructed from SH degrees 15–65 of the internal part of the CM4 model (Sabaka et al. 2004), and assuming zero external field contamination. The resulting artefacts take

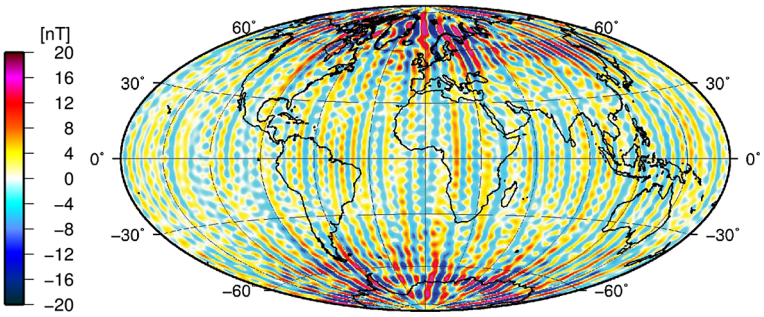

Fig. 4 Artefacts introduced into B_r in an internal field model, as a by-product of track-by-track external field estimation, due to self-contamination. This result is based on synthetic data and derived using Eq. (24)

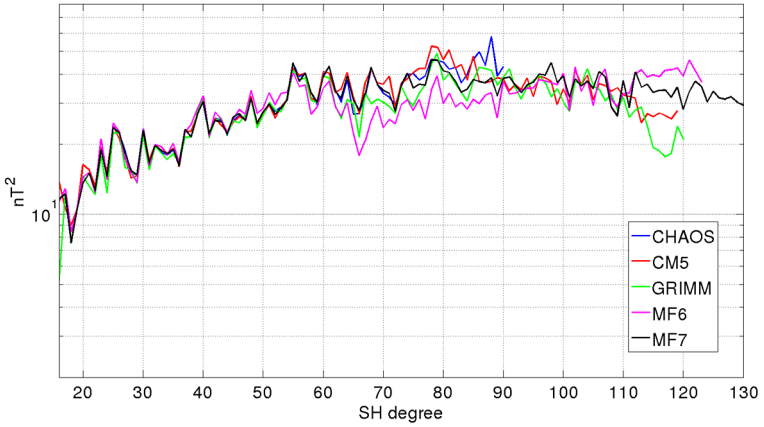

Fig. 5 The SH power spectra of the lithospheric field models MF7 (*black line*), MF6 (*magneta*), CM5 (*red line*), GRIMM_L120 (*green line*) and CHAOS-4 (*blue line*)

the form of spurious North-South patterns and reach 5–10 nT over the oceans. Experiments with the GRIMM field model (Lesur et al. 2008) using real data show that such artefacts can in some circumstances reach even larger values (see their Fig. 9). Of course, these artefacts also unavoidably distort by-products of lithospheric field models, such as magnetization or magnetic thickness maps.

There are several possible approaches to deal with the aforementioned problems. In the context of the track-by-track analysis method, the best strategy for minimizing leakage from the other sources is to have all field sources co-estimated from the same data set. In a sequential approach, in order to avoid the self-contamination by the lithospheric field, it is advisable to remove a lithospheric field model prior to performing track-by-track analysis and then to add it back.

A widely-used lithospheric field model series that makes extensive use of the track-by-track analysis is the MF series. For the latest published description see Maus et al. (2008); the most up-to-date version, MF7, is available online. In the construction of MF7, a main field model, an external field model and a lithospheric field model are co-estimated from the input data set, prior to the application of the track-by-track analysis and correction. Figure 5 shows the power spectra of MF7 (black curve) and its previous version, MF6 (Maus et al. 2008) (magenta curve).

An approach adopted by some workers is to deviate from a pure track-by-track analysis and to consider more data (i.e. more orbits) when estimating the external field model. More detail about how this is achieved when co-estimating an external field model is given in Sect. 3.2 above. As an example, the CHAOS series of models adopts this approach; in estimating the lithospheric field part of CHAOS-4 bins of 5 days were used to determine the external dipole in solar magnetic co-ordinates, while bins of 30 days were used for the order $m = 1$ terms. The power spectrum from CHAOS-4 is the blue line in Fig. 5.

A different approach has been followed in the framework of the latest GRIMM lithospheric field model GRIMM_L120 (Lesur et al. 2013). The rapidly-varying external field contribution is removed from a prototype lithospheric field model by means of a post-processing scheme. Details of this method are described in the paper by Thébault et al. (2016a) in this volume. The power spectrum of this model is shown in green in Fig. 5.

Another possible remedy, although not always achievable in practice, is to sample more than one longitude when estimating the external field coefficient q_1^0. It can be shown (see Eqs. (16) and (17) of Thébault et al. 2012) that the error term cancels out when the longitude at a given time is adequately sampled for a given degree w. Multi-satellite configurations, such as ESA's *Swarm* mission (e.g. Friis-Christensen et al. 2006), are needed to exploit this fact. Motivated by such a scenario, and also making use of simultaneous data from ground observatories spanning a range of longitudes, the latest version of the CM model series, CM5 (Sabaka et al. 2015), uses bins of data gathered within one hour for the estimation of the magnetospheric coefficients of SH degree one Sabaka et al. (2015). The power spectrum of CM5 is shown in Fig. 5 (red curve).

Overall, Fig. 5 illustrates that the present generation of lithospheric field models agree very well up to SH degree 60. The power spectra of lithospheric part of CHAOS-4, CM5, GRIMM_L120 and MF7 are also in close agreement up to approximately SH degree 85, while MF6 deviates significantly from them between SH degrees 60 and 90. We note, moreover, that MF7 is at present the lithospheric field model extending to the highest spherical harmonic degree (i.e. with the highest spatial resolution).

It is clear that great care is required in lithospheric field modelling when accounting for rapid magnetospheric variations. Track-by-track analysis can easily introduce artefacts into lithospheric models due to leakage of unmodelled sources present in the data. Despite these known problems, some such analysis to determine the rapidly varying magnetospheric field is unavoidable if one wishes to determine high degree lithospheric field. Many workers compromise and continue to employ some variant of the method. Best practice involves modelling and removing all other field sources using the same data set prior to modelling the magnetospheric field and its induced part (including a prototype lithospheric field model) but this procedure is always imperfect. On the other hand, the approach of using data from more than one satellite track to estimate the magnetospheric field does not have sufficient time resolution to enable one to track the true magnetospheric variations. Due to these limitations, the small scales of present lithospheric field models should be interpreted with some caution. Regarding the future, simultaneous monitoring of the magnetic field at multiple longitudes, by multi-satellite missions such as *Swarm*, offer a possible route towards improved models. Initial results using across-track differences from *Swarm* seem to be encouraging (Olsen et al. 2015; Thébault et al. 2016b).

5 Separation of the Ionospheric Field and Related EM Induction Effects from the Internal Field

The need to handle rapidly-varying magnetospheric fields, and difficulties with track-by-track analysis schemes, are a serious problem when modelling the high degree lithospheric

field. But since they involve leakage into the small-scale internal field, they are not the primary limiting factor regarding the determination of the large-scale internal (core) field and its time variations. Here, the major challenge comes from incomplete modelling of the field of ionospheric origin. The ionospheric field also varies rapidly in time, and includes spatial scales that overlap with those of the Earth's internal field. By ionospheric field, we shall mean the field generated by electrical currents within the ionospheric electrically conductive layer between about 80 and 200 km altitude. These currents, created by solar heating and tidal forcing, generate daily, seasonal, and annual magnetic field variations that fluctuate with the geomagnetic field and solar activity. In this section, we discuss the ionospheric field at non-polar latitudes. The more complex situation at polar latitudes, where magnetospheric-ionospheric coupling currents and their closure in the ionosphere play a crucial role, is described next in Sect. 6.

Models of the ionospheric field derived from geomagnetic field observations are typically time-averaged models (with dependence on season and solar activity level sometimes included) that describe only the so-called Solar Quiet (*Sq*) field (e.g. Richmond and Thayer 2000). The *Sq* currents generate magnetic fields of between 10 and 50 nT at the Earth's surface at magnetic latitudes below about ± 55 degrees that increase from sunrise to noon and decrease from noon to sunset. The *Sq* current system is characterized by two vortices facing the Sun in the Northern and Southern hemisphere that are separated by the equatorial electrojet (EEJ) flowing eastward along the geomagnetic dip equator within a latitudinal band of ± 5 degrees. The spatial variations of the *Sq* currents are therefore complex and their time variations induce electric currents within the Earth's lithosphere and mantle that superimpose on both the primary *Sq* field and on the core-generated internal field and its secular variation. In general, spherical harmonic models of the *Sq* ionospheric field are built upon the assumption that the electrical currents flow in an equivalent thin sheet in the E-region at an average altitude of about 110 km (e.g. Chulliat et al. 2013; Sabaka et al. 2015) and they rely heavily on magnetic observatory measurements that allow a mathematical separation between the primary external, and secondary internal (induced), magnetic fields.

Mathematically speaking, models of the ionospheric *Sq* field are usually derived in a magnetic coordinate system, such as the quasi-dipole system (e.g. Laundal and Richmond 2016). Readers are referred to Sabaka et al. (2002, 2015) and Chulliat et al. (2013) for the full details of the parameterization of ionospheric *Sq* fields and related induction effects, which we shall not attempt to adumbrate here.

Unfortunately, the global observatory network is not sufficiently dense to allow a source field separation in spherical harmonics to high spatial resolution. Low-Earth-Orbit (LEO) satellites, such as the *Swarm* constellation, collect homogeneous magnetic field measurements with a dense coverage. However, they measure the field well above the conductive ionosphere so that the primary and secondary Sq ionospheric fields are both internal to the satellite orbits. This configuration precludes the separation of the field into its primary and induced parts without additional information about the electrical conductivity structure of the solid Earth. We thus presently face a very difficult situation. On the one hand, observatory measurements allow a separation between primary and secondary ionospheric fields. But, to date, this separation allows us to infer the 3D electrical conductivity structure of the Earth's mantle (see e.g. Kuvshinov 2015, for a review) only at a spatial resolution too low to account for the spatial complexity of the induced ionospheric *Sq* field. On the other hand, although LEO satellites provide dense and homogeneous measurements, they fly above the *Sq* sources and a source field separation is not achievable without an accurate prior 3D electrical conductivity model.

Since the ionospheric *Sq* field is maximum at noon and minimum at midnight at mid-to-low latitudes, a common practice when constructing models of the internal geomagnetic

field is to simply select measurements from dark times, aiming to minimize leakage from the ionospheric field into the internal field models (e.g. Lesur et al. 2010; Maus et al. 2010; Finlay et al. 2015). The selection of data from dark regions reduces the small scale contributions of the ionospheric *Sq* field but does not correct for the night side primary field or the magnetic field induced in the mantle by the primary field on the day side (e.g. Olsen et al. 2005). In principle, the spatial structures of the ionospheric *Sq* field on the night-side may have less complexity than those in the day-side, so a 3D mantle conductivity model with low spatial resolution may arguably be sufficient to describe the large scale signatures induced by the primary ionospheric field.

Figure 6 illustrates the challenges currently faced by internal field modellers in handling the ionospheric field. It compares, at the Earth's mean spherical surface at epoch 2010.0, the vertical component of three candidate models submitted to IGRF-12 (Thébault et al. 2015b), and the final DGRF-2010 model that was included in IGRF-12. This was computed from the weighted average of 7 candidate models (Thébault et al. 2015a). The difference between the IGRF-12 model and Model 1, which was derived without data local time selection, shows small scale signatures with structures characteristic of the equatorial electrojet (EEJ) ionospheric field at noon local time (Fig. 6, top). The difference between the IGRF-12 model and Model 2, which sought to explicitly remove the ionospheric night-time primary and induced contributions, exhibits large-scale structures (Fig. 6, middle). A spectral analysis showed that these structures arise mostly from differences at SH degree 1 and 3 and at order 0 (Thébault et al. 2015a, their Fig. 2). Finally, the difference between the IGRF-12 model and Model 3 that relied only on night-side measurements selected at magnetically quiet times, does not exhibit specific large scale signatures (Fig. 6, bottom). It is important to stress that the relatively small difference for Model 3 may simply reflect the fact that the majority of candidate models used to construct the IGRF-12 model relied on a similar selection procedure. In particular, although it seems likely that Model 1 is contaminated by the EEJ field, it is currently very difficult to decide which of Model 2 and Model 3, based on different compromises, provides the best representation of the Earth's internal field.

6 Problems at Polar Latitudes: Unmodelled Fields Dependent on Quasi-Dipole Latitude and Magnetic Local Time

In this section we move on to discuss difficulties that occur when attempting to isolate the internal field at polar latitudes. Here, magnetosphere-ionosphere coupling currents (sometimes also referred to as field-aligned currents or Birkeland currents), and their closure currents in the ionosphere, produce strong and highly dynamic disturbance fields. We present the structure of these unmodelled disturbance fields in the polar regions, and highlight a danger that they may under some circumstances leak into the estimated internal field.

6.1 Polar Residuals from Internal Field Models

A useful approach in identifying possible shortcomings in geomagnetic field models is to look for structure in their residuals (input observations minus field models predictions). In this section we report on an investigation of residuals for scalar data from polar latitudes that were used to derive the CHAOS-5 field model (Finlay et al. 2015).

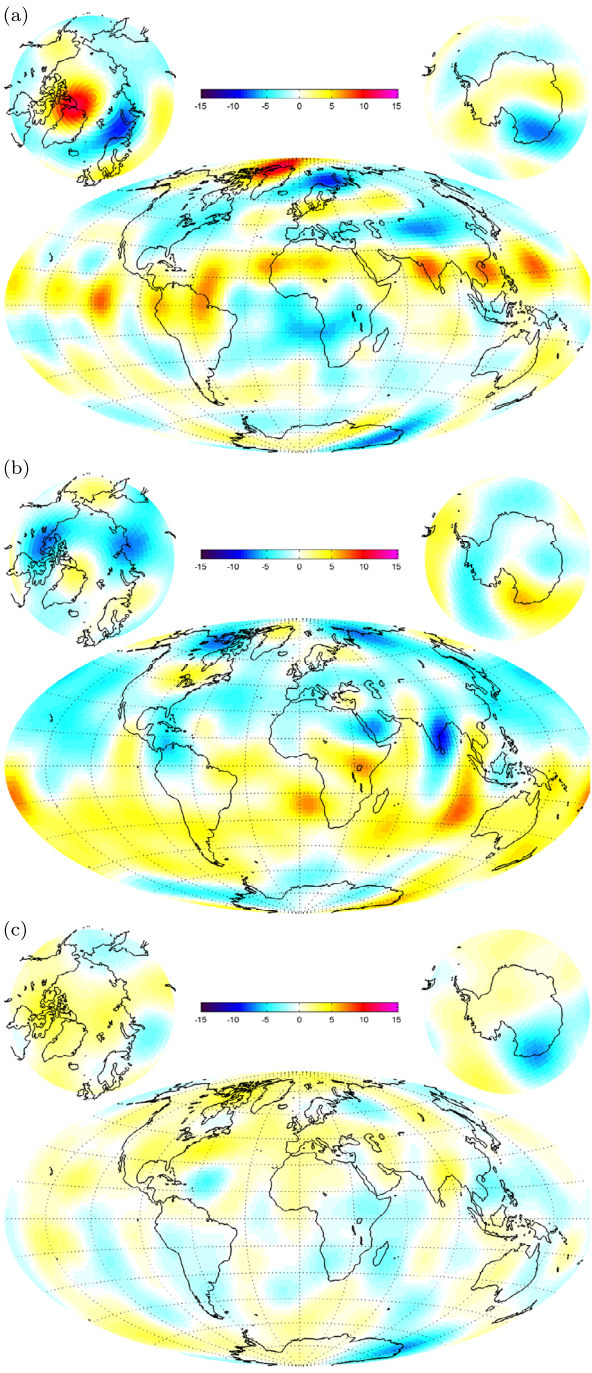

Fig. 6 Differences between candidate field models for IGRF-12 with different treatments of the ionospheric field and related induction, and the final IGRF-12 model, for epoch 2010.0. (**a**) Model 1, including data from both dark and sunlit regions, with no co-estimation of the ionospheric field; (**b**) Model 2 including data from both dark and sunlit regions, with co-estimation of the ionospheric field and related induction; (**c**) Model 3 including only data from dark regions, and with no co-estimation of the ionospheric field

Preliminary investigations of residuals of CHAMP and *Swarm* data, suggested an organization in a quasi-dipole (QD) latitude (Richmond 1995) and magnetic local time (MLT) (e.g. Sabaka et al. 2002) coordinate system. For a review of these and other related mag-

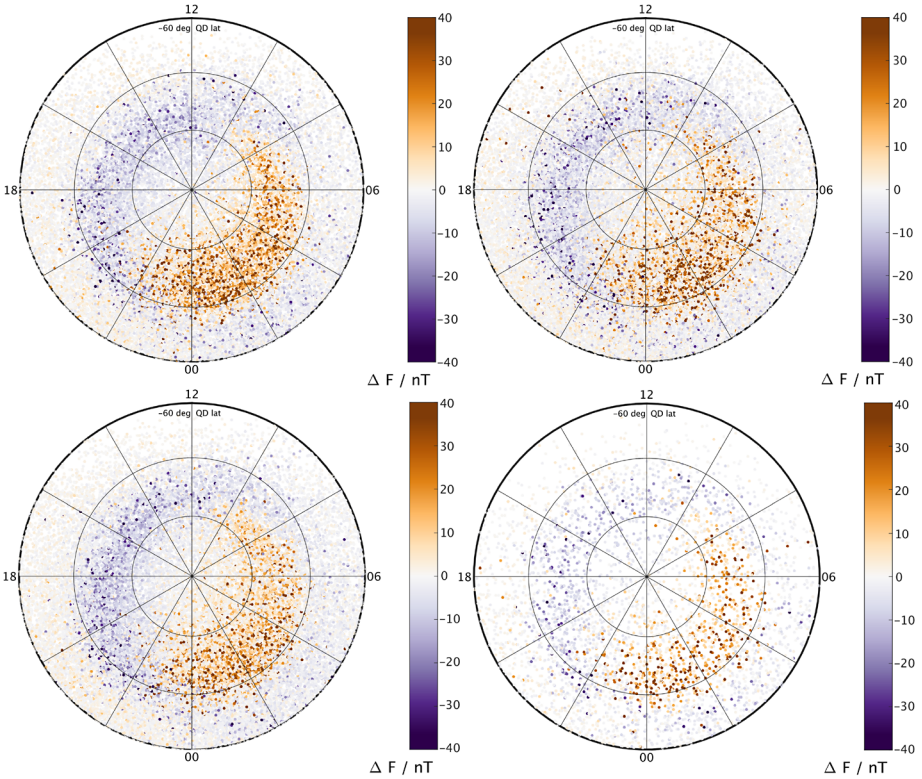

Fig. 7 Scalar field residuals of CHAMP data collected in the Southern polar region, as used in the CHAOS-5l field model (Finlay et al. 2015), arranged by the *IMF* clock angle. Displayed are residuals as a function of QD latitude and magnetic local time. The scale of ±40 nT is saturated. Note that due to selection of only dark data (sun at least 10 degrees below the horizon) some regions towards noon contain no data. Top left: IMF clock angle θ_{IMF} around −90 degrees (between −135 and −45 degrees); top right: *IMF* clock angle θ_{IMF} around 0 degrees (between −45 and +45 degrees); bottom left: *IMF* clock angle θ_{IMF} around 90 degrees (between +45 and +135 degrees); bottom right: *IMF* clock angles θ_{IMF} around 180 degrees (between 135 and −45 degree). The *black circles* delimit QD latitudes of 60, 70 and 80 degrees

netic coordinate systems, see Laundal and Richmond (2016) in this volume. Such patterns in magnetic signals at polar latitudes are well known from studies of ground-based magnetic data (e.g. Friis-Christensen and Wilhjelm 1975; Weimer et al. 2010) which have emphasized the importance of the *IMF* in controlling the responsible current systems.

A similar approach to that taken in ground-based studies was therefore adopted here to study CHAMP magnetic field scalar residuals between 2000 and 2010 from CHAOS-5. We present only scalar residuals, since CHAOS-5 does not use vector data at high latitudes. Furthermore, CHAMP had a lower altitude than Ørsted, and *Swarm* has not yet descended to comparable altitudes, so CHAMP data provide most information on the ionospheric E-layer currents that are expected to dominate the scalar residuals (see Sect. 6.3).

Figure 7 presents the scalar residuals of CHAMP data in the Southern hemisphere, as a function of the *IMF* direction. More specifically, the 'clock' angle, $\theta_{IMF} = \arctan(B_Y/B_Z)$, has been used to split the residuals into four categories. All residuals for each category of *IMF* direction are displayed. Midnight magnetic local time is at the bottom of each plot, noon is at the top, dusk is to the left and dawn to the right.

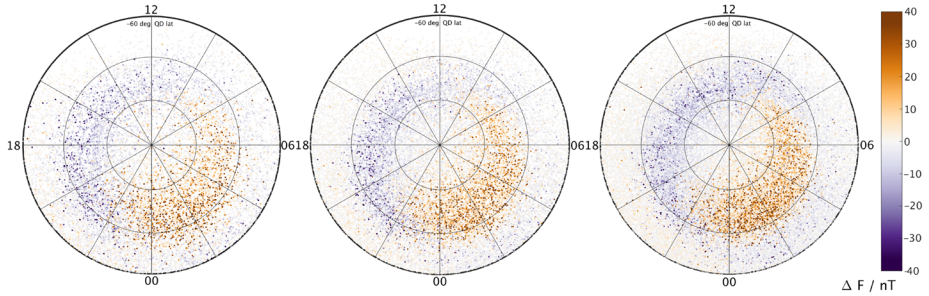

Fig. 8 Time-dependence of scalar field residuals from CHAMP data collected in the Southern polar region, as used in the CHAOS-5l field model (Finlay et al. 2015), for all *IMF* clock angles, before 2004.0 (left), from 2004.0 to 2007.0 (middle) and post 2007.0. Displayed are residuals as a function of QD latitude and magnetic local time. The scale of ±40 nT is saturated. Note that due to selection of only dark data (sun at least 10 degrees below the horizon) some regions towards noon contain no data. The *black circles* delimit QD latitudes of 60, 70 and 80 degrees

The scalar residuals presented in Fig. 7 are certainly not randomly distributed. The residuals show, to a first approximation, opposite signs for the morning and evening sectors, with the sign also changing as a QD latitude of approximately 70 degrees is crossed. Fewer data are selected for *IMF* clock angles close to 180 degrees in CHAOS-5, especially in the early years, though many of the residuals in this category have a relatively high amplitude. A rotation of the pattern of residuals is visible between *IMF* B_Y positive and negative (i.e. between $\theta_{IMF} \pm 90$ degrees). This has previously been seen in ground-based studies (e.g. Friis-Christensen and Wilhjelm 1975). Strong organization of horizontal field components minus field model predictions (not shown) is also found as a function of QD latitude and MLT; this is expected to be related to Region 1 and Region 2 field aligned currents (see Sect. 6.3).

One may be tempted to think that such a dependence on MLT is not a problem for internal field modelling, since during field model construction data from all MLTs are used, so the effects should average out. The problem is that LEO satellites only slowly change their MLT (for CHAMP 24 hours of local time was covered in about 8 months). This means there could be a bias resulting from sampling only a limited range of MLT at a certain QD latitude, if one considers short time-windows. This presents a major difficulty when seeking to determine rapid secular variation. In addition, it should be remembered that solar wind conditions are constantly evolving, and because of the selection criteria adopted in internal field modelling it is not obvious that the influence of the polar currents will ever completely average to zero.

It is also of interest whether or not the patterns of residuals presented in Fig. 7 are static or whether they exhibit some time-dependence. Figure 8 presents similar patterns of scalar residuals (but now considering all selected *IMF* conditions) for time windows of 2000–2004, 2004–2007 and 2007–2010. We find that in general more 'quiet-time' data are selected in the latest years, when solar activity was remarkably weak. Furthermore the signature of the polar cap currents is clearer during the later years, most likely because CHAMP was then at its lowest altitudes, closest to the ionospheric E-layer currents. The strongest field perturbations extend to slightly lower QD latitudes in the earlier years, when solar activity was higher and CHAMP was at a higher altitude.

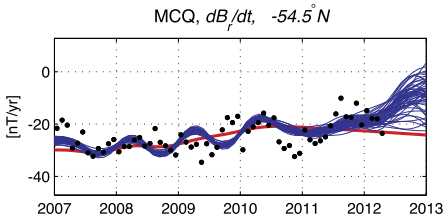

Fig. 9 An example of the influence of polar disturbances on the radial component of secular variation (dB_r/dt) as predicted by an ensemble of weakly regularized field model (*blue lines*) and a model with relatively strong temporal regularization imposed (*red line*, CHAOS-5l), focusing on the period 2007–2013. Only Ørsted, CHAMP, SAC-C and ground observatory data were used to constrain the blue models, hence their divergence towards the end of the interval (*Swarm* data was also used in CHAOS-5l (the *red line*)). Predictions are plotted at the site of the Macquarie Island (MCQ) observatory (latitude 54.5 degrees South, and QD latitude 64.2 degrees South). Annual differences of revised monthly mean observatory data (Olsen et al. 2014) are shown as *black dots*

6.2 Spurious SV in Time-Dependent Internal Field Models with Insufficient Temporal Regularization

The above discussion of systematic patterns in scalar residuals from the polar regions suggests the possibility of leakage from the magnetic signatures of polar currents into time-dependent field models. Is there any evidence for such a problem?

It is well known to those constructing time-dependent internal field models that strong temporal regularization must be applied during construction of models built from LEO satellite data, despite the excellent geographical coverage of the data. Otherwise, spurious short-period oscillations will result. The type of problems that occur can be readily identified in weakly regularized models that are not usually published. It turns out that strong temporal oscillations are seen especially in the zonal spherical harmonics, and their signature is strongest at auroral latitudes. As an example, in Fig. 9 we compare the secular variation (first time derivative of the field) predicted at Macquarie Island (MCQ) observatory from an ensemble of weakly regularized field models, constructed with a regularization matrix based on AR2 temporal covariances as advocated by Gillet et al. (2013) and a 6 month spline knot spacing, compared to the more heavily regularized CHAOS-5l field model over the period 2007–2013.

Spurious oscillations in the secular variation are found in the weakly regularized internal field models, particularly in the vertical component close to the auroral zone. These oscillations are of larger amplitude than the field change monitored by annual differences of ground observatory monthly means in the auroral zone. In the example shown in Fig. 9, the oscillations seem to have a period of close to 1 year, and they are not in phase with signals from the ground observatory. It seems likely they result from a combination of annual variations in the data coverage (for example due to the dark selection criteria used in the models presented here), and perhaps also from annual variations of the coherent patterns shown in Fig. 7, due to changes in the ionospheric conductivity, and magnetosphere-ionosphere coupling currents, with season. It is noteworthy that patterns in the polar residuals as a function of QD latitude and MLT are also seen for models such as GRIMM (Lesur et al. 2008) that use different selection criteria, and are not restricted to scalar data in the polar regions.

The usual approach to handle this problem is to enforce strong temporal regularization of time-dependent field models. However, this is unsatisfactory since it also smooths out real secular variation signals of interest, in particular at mid and low latitudes, that are not

connected to the problems in the polar regions. Clearly new strategies are needed to better handle these unmodelled signals at polar latitudes in order to improve our probing of rapid core dynamics.

6.3 A Physical Interpretation of the Origin of Unmodelled Signals at Polar Latitudes

It is certainly of interest to try to understand the physical origin of the polar residual patterns presented in Fig. 7. If they can be understood, perhaps their influence can be mitigated or they can be co-estimated and removed. Below we present an overview of basic polar electrodynamics, along with some suggestions for the possible origin of the observed polar residuals. A more detailed and nuanced discussion can be found in the article by Friis-Christensen et al. (2016) in this volume.

A crucial process in determining the structure of polar current systems and related magnetic disturbances is the large-scale magnetospheric circulation known as the Dungey cycle (Dungey 1961), and its associated coupling to the conductive ionosphere. The Dungey cycle arises from the following principles. In a collisionless plasma, the charged particles may be thought of as being 'frozen' into the magnetic field lines. This is the case for both the solar wind and the Earth's magnetic field in space. They therefore resist mixing, and the solar wind deforms the terrestrial magnetic field, shaping the magnetosphere (e.g. Cowley 2007). However, the frozen-field conditions do not always apply. When the interplanetary magnetic field is orientated southwards ($IMF\ B_Z < 0$), the solar and terrestrial magnetic fields can merge in a process called magnetic reconnection (e.g. Baumjohann and Treumann 1997). This creates 'open' field lines in the region of the polar cap, with one end connected to the Earth and the other end in the solar wind (Kelley 2009). The motion of the solar wind pushes the open field lines from noon towards midnight over the polar cap, where they re-join the closed magnetosphere via nightside reconnection in the magnetotail. The newly-closed field lines complete the cycle by returning to the dayside at lower latitudes, approximately aligned with the auroral oval (Kivelson and Russell 1995). At the same time, the motion of the open field lines through the resistive ionosphere is thought to induce an effective electric field across the polar cap, directed from dawn to dusk while the return motion of the plasma along with closed field lines at auroral latitudes is thought to produce an effective electric field directed from dusk to dawn (see Fig. 10).

Since the ionospheric plasma is undergoing collisions with neutral particles, it has an anisotropic conductivity distribution, which adds further complexity to the currents arising from the Dungey cycle. Currents perpendicular to the magnetic field and in the direction of the plasma-convection induced electric field are termed Pedersen currents; those perpendicular to both magnetic and the electric fields are called Hall currents (Rishbeth 1988). The Hall conductivity peaks around 110 km altitude, and Pedersen conductivity around 125 km, hence the different currents have contributions from particle populations of differing mean energies. The large-scale effective electric fields induced by the Dungey cycle create a system of currents which are closed via the Region-1 and Region-2 (R1, R2) field-aligned (Birkeland) currents, as shown in Fig. 10a. The closure of the R1 current system is thought to occur across the magnetopause (opposing the typical Chapman-Ferraro current direction), while the R2 system is thought to close via the ring current (Lockwood 2013; Coxon 2015). At ground level (assuming radial field-aligned currents with no gradients in ionospheric conductivity), the magnetic perturbations due to curl-free horizontal currents and those due to the field-aligned currents will exactly oppose according to Fukushima's theorem (Fukushima 1976), in which case only the magnetic signatures of divergence-free

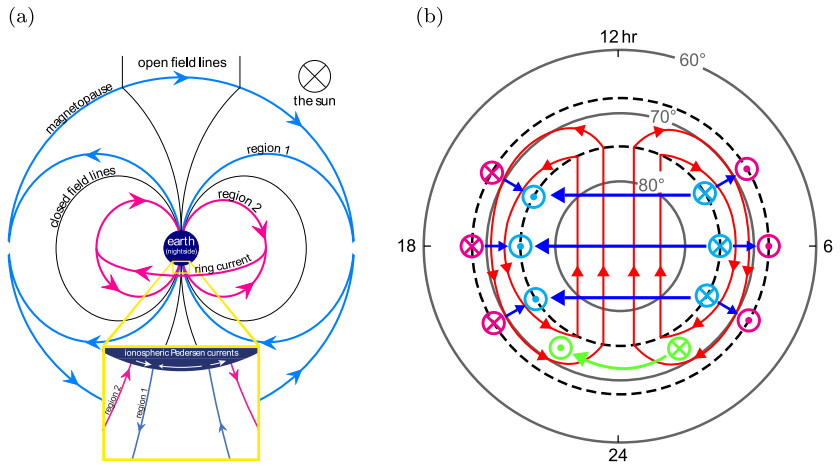

Fig. 10 Panel (**a**) shows the current system associated with the Dungey cycle, illustrating the closure paths of the region 1 and region 2 field-aligned (or Birkeland) currents. From Coxon (2015). Panel (**b**) shows the polar ionospheric 'footprints' of the currents depicted in panel (a). The region 1 and region 2 field-aligned currents are shown in *light blue* and *pink* respectively. Currents directed into the ionosphere are shown as *crosses*, and currents out of the ionosphere as *dots*. Suggestions for the horizontal Pedersen and Hall currents driven by plasma convection are shown as *blue* and *red arrows* respectively. The *inner dotted line* corresponds to the boundary of the open field lines (i.e. the polar cap), and the *outer dotted line* is the equatorward edge of the auroral oval. The substorm current wedge is shown in *green*. Adapted from Kelley (2009), Lockwood (2013) and Coxon (2015)

horizontal currents will be observed. However, at satellite altitude (above the majority of the ionosphere) the magnetic perturbations resulting from the curl-free horizontal current can act to reinforce the magnetic signature of the field-aligned currents. Considering the radial (or scalar) field magnetic perturbation at satellite altitude, horizontal currents flowing through the conducting auroral oval are expected to make the largest contribution. The following summary of the expected and observed distribution of the magnetic residuals follows from the illustration in Fig. 10b.

The pattern of the observed scalar magnetic residuals in Fig. 7 along the dawn-dusk meridian changes sign in the centre of the auroral oval, and has noticeably weaker amplitude inside the polar cap, as expected for the magnetic signature of horizontal currents flowing along the auroral oval, and as illustrated in Fig. 10b. Note the unexpected asymmetry in the magnitude of the scalar residuals about the noon-midnight meridian: those on the dawnside are much stronger. This may be a consequence of the imperfect data selection criteria used in CHAOS-5 (and other internal field models), where it is difficult to exclude substorms that often involve an enhanced substorm current wedge, located close to midnight and seen most clearly in the morning sector. Friis-Christensen et al. (2016) discuss in detail the interplay between the magnetic signatures of plasma-convection driven currents and the substorm wedge currents, as well as the importance of IMF B_Y in modulating these processes. The stronger dawnside residuals may also partly reflect particle precipitation processes. The Dungey convection does not depend on the energy of the particles, but curvature and gradient drifts do (pp. 16, 17, 20 Baumjohann and Treumann 1997). Hence, lower energy particles (which contribute to Pedersen conductivity) will follow the Dungey convection more closely than high-energy particles, which will be more strongly controlled by magnetic drifts. Specifically, high energy electrons are expected to drift towards the dawn sector in the magnetosphere (Kivelson and Russell 1995, p. 465, Fig. 14.3(a)). Ions drift in

the opposite direction but have a lower chance of precipitating and are more susceptible to collisions with neutrals, which lowers the ion current (Kivelson and Russell 1995, p. 326), hence there is a possibility this could contribute to a dawn-dusk asymmetry in horizontal currents.

The scalar residuals in Fig. 7 are presented for a specific IMF clock angle. Examples of how the ionospheric electrodynamics alter in shape and magnitude with *IMF* clock angle are given by Weimer (2005) and Weimer (2013). Whilst the internal field geometry (i.e. QD coordinates) is certainly a reasonable system for organising the magnetic signatures of polar currents, dynamic behaviour in the both the centroid and latitudinal extent of the auroral oval are to be expected, according to the continually fluctuating dayside and nightside reconnection rates. This is known as the Expanding-Contracting Polar Cap (ECPC) paradigm (Cowley and Lockwood 1992). Additional modulation of the currents is also to be expected according to season; Guo et al. (2014) provide a good example in their Fig. 2. Seasonal variations in the polar currents are at least partly due to variations in solar radiation-based polar ionospheric conductivity, as well as the increased likelihood of southwards *IMF* at equinox due to the Russell-McPherron effect (Russell and McPherron 1973).

Given the dynamic nature of polar electrodynamics, the global network of ground-based observatories and variometers provide very important information for studies of polar current systems. However, according to Fukushima's theorem only the divergence-free horizontal current (which is often interpreted as a Hall current) can be measured at ground level. Recent research (Laundal et al. 2015) has confirmed earlier ideas (Vasyliunas 1970) that the field-aligned currents can (indirectly) affect the relative contributions of the horizontal currents to the magnetic signal measured at ground. Linking ground-based measurements of the polar currents to the perturbations at satellite altitude in general depends on knowledge of the ionospheric conductivity distribution, which is not well constrained.

Although the broad statistical character of the observed polar residuals can be described in terms of plasma convection (the Dungey cycle) and the substorm current wedge (associated with ionosphere-magnetosphere coupling), a detailed understanding of residual amplitudes on an event-by-event basis remains challenging. A particular problems is that whilst the dayside and nightside reconnection rates are expected to balance over long time spans, the nightside reconnection rate (in the form of substorms) is much more stochastic than the comparatively steady dayside reconnection.

7 Discussion and Concluding Remarks

7.1 Quiet-Time Data Selection

The difficulties discussed above are all linked either to the leakage of magnetospheric or ionospheric fields (and related induced signals) into internal field models, or to problems inadvertently introduced by schemes designed to mitigate such effects. The severity of the problems, and the need for (possibly dangerous) corrections, would of course be reduced if there were more effective ways to identify 'quiet' times. It is therefore worth pausing at this stage to reconsider the selection criteria typically adopted in internal field modelling, and to reflect on how these might be improved upon.

A general problem with using indices to define 'quiet' levels is that they are necessarily imperfect proxies for idealized physical processes. For example, *Dst* and related indices, designed to monitor the magnetospheric ring current, contain the signatures of other current systems (e.g. tail currents), and only provide information on symmetric field disturbances

on hourly time scales. As another example, K_p gives range information averaged over its contributing sites, that are found mostly at northern mid-latitudes at only a three hourly resolution. Neither index provides information on local-time dependent processes including magnetospheric-ionospheric coupling processes, and related ionospheric currents, that may have consequences, even at mid latitudes, for data collected by LEO satellites.

Considering higher latitudes, selection criteria involving the *IMF* B_Z and B_Y components are much used for data selection, but large amplitude disturbances nonetheless remain in the selected 'quiet' time data. The analysis of scalar field residuals in the polar regions, for example from CHAOS-5 as presented in Sect. 6, generally show slightly larger amplitudes when *IMF* B_Z is negative, particularly in the post-midnight morning sector, consistent with enhanced substorm current wedge activity. There is also an asymmetry in the residuals observed when *IMF* B_Y is positive compared to negative (see Friis-Christensen et al. 2016, in this issue for more details). Short period changes in the *IMF* can cause intense field perturbations in the polar regions that may be delayed by an hour or more on the night side, due to the complexity of loading and unloading processes in the tail. Due to the unpredictability of nightside reconnection it is at present difficult to completely remove substorms events using measurements of the solar wind, and the *IMF*. It might nonetheless help in removing some badly disturbed events if one were to exclude data for which there has been a large change in the *IMF* in the proceeding few hours, or for which *IMF* B_Z negative (or large amplitude *IMF* B_Y) occurred within the preceding few hours. In this regard, it is worth noting that large changes in the *IMF* can occur on time scales as short as a few minutes (Friis-Christensen et al. 2016). Looking at other solar wind parameters, such as the solar wind flow pressure or proton particle density, may also provide additional constraints.

A more subtle, and possibly even more serious effect within the framework of secular variation modelling, is the possibility of time-varying biases in the distribution of high latitude disturbance fields, that could leak into the internal field. Here avoiding trends in the statistics of unmodelled fields is important, but these are difficult to diagnose. As an example, selecting data according to a chosen threshold value of K_p results in more data being accepted as solar minimum is approached, despite the fact that the selected data contain considerable disturbance fields at polar latitudes, which are statistically correlated as function of QD latitude and MLT. Further study of such issues is certainly required.

There is currently no consensus on how to handle data selection in sunlit polar regions. Larger amplitude currents, with higher spatiotemporal complexity, are expected in the sunlit polar ionosphere due to its higher conductivity, which provides additional pathways to couple with (i.e. short-circuit) various magnetospheric processes. The signatures of these large amplitude currents (and their seasonal variations) must be dealt with, for example using model regularization, if data from the sunlit polar regions is selected. On the other hand, if only dark data is used this leads to annual variations in the amount and geographic distribution of the data, which is a serious problem if one wishes to build global spherical harmonic models with time-dependence on sub-annual timescales. Semi-annual variations in the activity of polar cap currents are also expected, with gradients in the insolation across the polar cap tending to maximise at the same time as the Russell-McPherron effect, leading the equinoxes to be substantially more complex and dynamic than either of the two solstices. How best to handle such variability is by no means obvious at present.

One possible route to improved data selection may be more direct use of near-Earth magnetic data, from LEO satellites, and data from ground observatories and variometers, rather than relying on global indices (see e.g. Thomson et al. 2010). For example, data from the SuperMAG (http://supermag.jhuapl.edu/) network at nearby QD latitudes and MLT could conceivably be used to better identify and exclude large amplitude disturbances at

polar latitudes. It might also be worth looking closely at the horizontal field components in satellite data when determining whether or not to accept scalar data in the polar regions, since perturbed horizontal components (due to strong field aligned currents) are likely to be associated with enhanced horizontal currents that will also disturb the scalar data.

Of course, it is impossible to entirely avoid unmodelled magnetospheric and ionospheric fields by means of data selection. The aim should rather be to identify, as far as possible, consistent sets of data without trends and biases, that are compatible with the parameterized fields fit to the data, and with the assumptions made regarding the statistics of the unmodelled fields during the model estimation process.

7.2 Alternative Field Parameterization Schemes

Solutions to the problems described above will also require new approaches to the separation of contributions from different sources. A system of representation of the external fields is therefore needed that contains enough information on the origin of the fields that internal and external contributions to magnetic data separate naturally, even with a relatively small number of data points. In this article we have focused on the most common technique of representation of the geomagnetic fields, based on SH expansions, but other methods for modelling these fields have also been proposed. The SH based methods originate form C.F. Gauss' work in the middle of the 19th century. It was already clear at that time that SH could be used to model fields of internal and external origins.

As explained in Sect. 3.2 the first acceptable external field models were obtained from Magsat satellite data. At around the same time, in order to deal with the inhomogeneous geographical distribution of ground observatory data, Shure et al. (1982) introduced harmonic splines. This was originally used an interpolation technique on the sphere, that could handle vector data; it therefore has as many parameters as sampling points (see also Wessel and Becker 2008). The technique has not often been used, in part because it does not provide a direct way to separate external and internal contributions to the magnetic field. The same difficulty arises for many local representation techniques (see for examples the review in Schott and Thébault (2011)). All these techniques therefore require pre-processing steps to remove from the data contributions from unwanted sources; this must be carried out using other approaches. One exception is the work by Mayer and Maier (2006) where vector wavelets are defined for both internal and external sources, enabling a separation of the associated signals.

Localised techniques have proven useful in the analyses of sources for which short spatial wavelengths contributions dominate, such as lithospheric or ionospheric fields. Closely related to harmonic splines, the representer technique described by (Parker 1994), considers the problem from the viewpoint of inverse theory (although the problem of how to separate fields of internal and external origin is not discussed). The representer technique has been applied by Whaler and Langel (1996) and Whaler and Purucker (2005) to model lithospheric fields. Focusing on core fields averaged over relatively long time-intervals, and using data that were pre-processed to remove as far as possible the signatures from unwanted sources, Constable et al. (1993) and Jackson et al. (2007) adopted a related approach based on a localized representation on the core surface. Although the functions used by Constable et al. (1993) are in many aspects similar to those proposed by Shure et al. (1982), they are not presented as being reproducing kernels of an Hilbert space, nor as splines minimizing a given norm. As we discuss in more detail below, Holschneider et al. (2016) have recently gone one step further and shown that the harmonic splines can be considered as just one example of a correlation function in space.

Although harmonic splines and equivalent local formulations have been studied for several decades, modelling of the external field has usually been ignored. Holschneider et al. (2016) have recently presented a new formulation that handles both internal and external fields, showing that the harmonic splines are, under a particular set of hypotheses, simply correlation functions of the contributions to magnetic field observations at two different points in space. The correlation functions for the magnetic potentials between two points in space x and y, take the form:

$$\mathbb{E}\big[\Phi(x)\,\Phi(y)\big] = r_i^2 \sum_\ell \lambda_\ell^2\, P_\ell(\hat{x}\cdot\hat{y})\Big(\tfrac{r_i^2}{|x||y|}\Big)^{\ell+1}, \tag{25}$$

and

$$\mathbb{E}\big[\Phi(x)\,\Phi(y)\big] = r_e^2 \sum_\ell \lambda_\ell^2\, P_\ell(\hat{x}\cdot\hat{y})\left(\frac{|x||y|}{r_e^2}\right)^{\ell}, \tag{26}$$

for magnetic potentials of internal and external origins respectively. In these equations $\mathbb{E}[\cdot]$ is the expected value, $\hat{x}$ is $x/|x|$ and similarly for $\hat{y}$. P_l are the Legendre polynomials. The quantities r_i and r_e are reference radii for internal and external sources. The Gauss coefficients are assumed uncorrelated, have zero mean and have a given degree variance λ_ℓ^2:

$$\mathbb{E}[g_{\ell,m}] = 0, \qquad \mathbb{E}[g_{\ell,m}\, g_{\ell',m'}] = \lambda_\ell^2\, \delta_{\ell,\ell'}\, \delta_{m,m'}, \quad \text{for all } \ell, m, \ell', m'. \tag{27}$$

As in Shure et al. (1982) simple choices for λ_ℓ^2 lead to explicit expressions for Eqs. (25) and (26). Natural choices are $\lambda_\ell^2 = 1$, or $\lambda_\ell^2 = \frac{1}{\ell+1}$ for internal potentials and $\lambda_\ell^2 = \frac{1}{\ell}$ for external potentials. Taking the gradients of the two correlation functions (25), (26), relative to their two variables x and y, leads to harmonic splines. Therefore, properly scaled, harmonic splines are correlation functions for field components of internal and external origin. Holschneider et al. (2016) have recently demonstrated how these correlation functions can be used to model the global geomagnetic field.

Perhaps the most important result presented by Holschneider et al. (2016), is the possibility of separating the different contributions to magnetic measurements simply by imposing the reference radius and the degree variance scaling of the sources. There is no need to impose arbitrary temporal smoothing or a SH truncation degree on the expansion of the external field. Most other existing technique do not carry in their system of representation sufficient information about the sources of the magnetic field to separate the different contributions without introducing some additional smoothness hypothesis. In principle, this opens the way to a better control of leakage between contributions and also, through use of a Bayesian formalism, to proper estimates of the model variance. The reason both Mayer and Maier (2006) and Holschneider et al. (2016) are able to carry out an internal/external separation is that although they analyse the field with local functions they perform integrations on a global scale (over a closed spherical surface), which is a necessary condition for such a separation.

7.3 Prior Knowledge from Other Observations and Models

As emphasised in the previous section, in order to improve upon the existing generation of geomagnetic field models better advantage needs to be taken of all the information we have concerning the field sources, both modelled and unmodelled. Regarding the internal field, statistical prior information on the expected properties of the core field (from theory

or numerical dynamo models) could be included via model covariances matrices (see for example Fournier et al. 2007; Aubert 2013, 2014) or equivalently using correlation functions within the framework proposed by Holschneider et al. (2016). Eventually this may lead to an application of data assimilation methods directly on magnetic observations, which may aid the separation of the contributing sources. Use of the known large-scale core field as a constraint on the induced component of the lithospheric field may help in separating it into induced and remanent parts, as well as in identifying possible artefacts in lithospheric field models. Regarding the separation of the induced ionospheric field from the core field, improved models of the mantle conductivity would be of great benefit.

The parameterization of magnetospheric fields, and related magnetosphere-ionosphere coupling currents, in present field models is a very crude representations of the expected physics. It is likely that much could be learned from MHD forward models of this system, especially if these could have more focus on geomagnetically quiet times and a sufficiently accurate representation of the ionosphere. For now, such studies seem to have fallen into the gap between the internal and external field communities.

The problem with large amplitude unmodelled disturbances at polar latitudes, that presently hinder studies of both the small scale lithospheric field and rapid time variations of the core field, is another case where prior knowledge (for example the expected statistical patterns of scalar field disturbances produced by the horizontal currents flowing in the auroral oval) is largely ignored during internal field modelling. In this case it may be possible, with sufficient constraints on the structure of expected fields and use of suitable co-ordinate systems, to co-estimate the mean, or even the slowly time changing part, of the polar disturbance fields. On the other hand, how to deal with the very rapidly changing part of the polar disturbance fields remains an outstanding problem; solutions to this challenge will likely only be feasible as part of a renewed collaboration between the internal and external field communities.

Acknowledgements The authors are grateful to the International Space Science Institute for inviting them to take part in the workshop on "Earth's Magnetic Field" held in Bern in May 2015. CCF thanks Eigil Friis-Christensen and Karl-Magnus Laundal for helpful discussions. The results presented in this paper rely on data collected at magnetic observatories. We thank the national institutes that support them and INTERMAGNET for promoting high standards of magnetic observatory practice (www.intermagnet.org). The support of the CHAMP mission by the German Aerospace Center (DLR) and the Federal Ministry of Education and Research is gratefully acknowledged. *Swarm* L1b data were provided by ESA. We also wish to thank two anonymous reviewers for helpful comments.

References

J. Arkani-Hamed, L.A. Langel, M. Purucker, J. Geophys. Res. **99** (1994)
J. Aubert, Geophys. J. Int. (2013). doi:10.1093/gji/ggs051
J. Aubert, Geophys. J. Int. **197**, 1321 (2014)
W. Baumjohann, R. Treumann, *Basic Space Plasma Physics* (1997)
J. Bloxham, A. Jackson, J. Geophys. Res. **97**, 19537 (1992)
J.C. Cain, Z. Wang, C. Kluth, D.R. Schmitz, Geophys. J. **97**, 431 (1989)
A. Chulliat, S. Maus, J. Geophys. Res. **119**, 1531–1543 (2014). doi:10.1002/2013JB010604
A. Chulliat, P. Vigneron, E. Thébault, O. Sirol, G. Hulot, Earth Planets Space **65**, 1271 (2013)
A. Chulliat, S. Macmillan, P. Alken, C. Beggan, M. Nair, B. Hamilton, A. Woods, V. Ridley, S. Maus, A. Thomson, The US/UK World magnetic model for 2015–2020: technical report (2015)
F. Civet, E. Thébault, O. Verhoeven, B. Langlais, D. Saturnino, Geophys. Res. Lett. **42**(9) (2015)
C.G. Constable, R.L. Parker, P.B. Stark, Geophys. J. Int. **113**, 419 (1993)
S.W.H. Cowley, in *Encyclopedia of Geomagnetism and Paleomagnetism*, ed. by D. Gubbins, E. Herrero-Bervera (Springer, Berlin, 2007), pp. 656–664

S. Cowley, M. Lockwood, in *Annales Geophysicae*, vol. 10 (1992), pp. 103–115
J.C. Coxon, The role of Birkeland currents in the Dungey cycle. Ph.D. thesis, University of Leicester, Department of Physics and Astronomy (2015)
C. de Boor, *A Practical Guide to Splines*. Applied Mathematical Sciences, vol. 27 (Springer, New York, 1978)
J.W. Dungey, Phys. Rev. Lett. **6**, 47 (1961)
C.C. Finlay, N. Olsen, L. Tøffner-Clausen, Earth Planets Space **67**, 114 (2015)
A. Fournier, C. Eymin, T. Alboussière, Nonlinear Process. Geophys. **14**(3), 163 (2007)
E. Friis-Christensen, J. Wilhjelm, J. Geophys. Res. **80**, 1248 (1975)
E. Friis-Christensen, H. Lühr, G. Hulot, Earth Planets Space **58**, 351 (2006)
E. Friis-Christensen, C.C. Finlay, M. Hesse, K.M. Laundal, Space Sci. Rev. (2016), in review
N. Fukushima, Rep. Ionos. Space Res. Jpn. **30**, 35 (1976)
N. Gillet, D. Jault, C.C. Finlay, N. Olsen, Geochem. Geophys. Geosyst. **14**, 766–786 (2013). doi:10.1029/2012GC004355
J. Guo, H. Liu, X. Feng, T.I. Pulkkinen, E.I. Tanskanen, C. Liu, D. Zhong, Y. Wang, J. Geophys. Res. Space Phys. **119**(4), 3179 (2014)
B. Hamilton, Earth Planets Space **65**, 1295 (2013)
M. Holschneider, V. Lesur, S. Mauerberger, J. Baerenzung, J. Geophys. Res., Solid Earth **121**, 3142 (2016)
G. Hulot, T. Sabaka, N. Olsen, A. Fournier, The present and future geomagnetic field, in *Treatise on Geophysics*, 2nd edn. (Elsevier/Academic Press, Amsterdam/San Diego, 2015), pp. 33–78
A. Jackson, C. Constable, M. Walker, R. Parker, Geophys. J. Int. **171**(1), 133 (2007)
K. Kauristie, A. Morschhauser, N. Olsen, M.R.L. Finlay C. C, J.W. Gjerloev, H.J. Opgenoorth Space Sci. Rev. (2016), in review
M. Kelley, **96** (2009)
M.G. Kivelson, C.T. Russell, *Introduction to Space Physics* (1995)
P. Kunagu, G. Balasis, V. Lesur, E. Chandrasekhar, Geophys. J. Int. (2013). doi:10.1093/gji/ggs093
A. Kuvshinov, *Global 3-D EM Studies of the Solid Earth: Progress Status*, 2nd edn. (Elsevier, Oxford, 2015)
A. Kuvshinov, N. Olsen, 3-D modelling of the magnetic fields due to ocean tidal flow, in *Earth Observation with CHAMP*, ed. by C. Reigber, H. Lühr, P. Schwintzer, J. Wickert (Springer, Berlin, 2005), pp. 359–365
R. Langel, in *Geomagnetism*, vol. 1, ed. by J.A. Jacobs (Academic Press, San Diego, 1987), pp. 249–512
R. Langel, J. Geomagn. Geoelectr. **44**, 679 (1992)
R.A. Langel, R.H. Estes, J. Geophys. Res. **90**, 2487 (1985a)
R.A. Langel, R.H. Estes, J. Geophys. Res. **90**, 2495 (1985b)
R.A. Langel, R.H. Estes, G.D. Mead, E.B. Fabiano, E.R. Lancaster, Geophys. Res. Lett. **7**, 793 (1980)
R.A. Langel, C.C. Schnetzler, J.D. Phillips, R.J. Horner, Geophys. Res. Lett. **9**, 273 (1982)
R.A. Langel, T.J. Sabaka, R.T. Baldwin, J.A. Conrad, Phys. Earth Planet. Inter. **98**, 235 (1996)
K.M. Laundal, A.D. Richmond, Space Sci. Rev. (2016). doi:10.1007/s11214-016-0275-y
K.M. Laundal, S.E. Haaland, N. Lehtinen, J.W. Gjerloev, N. Ostgaard, P. Tenfjord, J.P. Reistad, K. Snekvik, S.E. Milan, S. Ohtani, B.J. Anderson, Geophys. Res. Lett. **42**, 7248 (2015)
V. Lesur, S. Macmillan, A. Thomson, Geophys. J. Int. **160**(1), 79 (2005). http://www.blackwell-synergy.com/doi/abs/10.1111/j.1365-246X.2004.02479.x
V. Lesur, I. Wardinski, M. Rother, M. Mandea, Geophys. J. Int. **173**, 382 (2008)
V. Lesur, I. Wardinski, M. Hamoudi, M. Rother, Earth Planets Space **62**, 765 (2010)
V. Lesur, M. Rother, F. Vervelidou, M. Hamoudi, E. Thébault, J. Geophys. Res., Solid Earth **4**, 105 (2013)
V. Lesur, M. Rother, I. Wardinski, R. Schachtschneider, M. Hamoudi, A. Chambodut, Earth Planets Space **67**, 87 (2015a)
V. Lesur, K. Whaler, I. Wardinski, Geophys. J. Int. **201**(2), 929 (2015b)
V. Lesur, M. Hamoudi, Y. Choi, J. Dyment, E. Thébault, Earth Planets Space **68**(1), 27 (2016)
M. Lockwood, Living Rev. Sol. Phys. **10** (2013)
H. Lühr, S. Maus, Earth Planets Space **62**, 843–848 (2010)
S. Macmillan, J.M. Quinn, Earth Planets Space **52**, 1149 (2000)
M. Mandea, I. Panet, V. Lesur, O. De Viron, M. Diament, J.L. Le Mouël, Proc. Natl. Acad. Sci. USA (2012). doi:10.1073/pnas.1207346109
S. Maus, Magnetic field model MF7 (2010). www.geomag.us/models/MF7.html
S. Maus, Geophys. J. Int. **203**, 1873 (2015)
S. Maus, H. Lühr, Geophys. J. Int. **162**, 755 (2005)
S. Maus, P. Weidelt, Geophys. Res. Lett. **31**, L12614 (2004). doi:10.1029/2004GL020232
S. Maus, M. Rother, R. Holme, H. Lühr, N. Olsen, V. Haak, Geophys. Res. Lett. **29**(10), 47 (2002)

S. Maus, H. Lühr, G. Balasis, M. Rother, M. Mandea, Introducing POMME, the POtsdam Magnetic Model of the Earth, in *Earth Observation with CHAMP*, ed. by C. Reigber, H. Lühr, P. Schwintzer, J. Wickert (Springer, Berlin, 2005), pp. 293–298. ISBN 978-3-540-22804-2
S. Maus, M. Rother, K. Hemant, C. Stolle, H. Lühr, A. Kuvshinov, N. Olsen, Geophys. J. Int. **164**, 319 (2006a)
S. Maus, M. Rother, K. Hemant, C. Stolle, H. Lühr, A.V. Kuvshinov, N. Olsen, Geophys. J. Int. **164**, 319 (2006b)
S. Maus, H. Lühr, M. Rother, K. Hemant, G. Balasis, P. Ritter, C. Stolle, Geochem. Geophys. Geosyst. **8**(5), Q05013 (2007)
S. Maus, F. Yin, H. Lühr, C. Manoj, M. Rother, J. Rauberg, I. Michaelis, C. Stolle, R.D. Müller, Geochem. Geophys. Geosyst. **9** (2008)
S. Maus, C. Manoj, J. Rauberg, I. Michaelis, H. Lühr, Earth Planets Space **62**, 729 (2010)
S. Maus, M. Rother, C. Stolle, W. Mai, S. Choi, H. Lühr, D. Cooke, C. Roth, Geochem. Geophys. Geosyst. **7**(7) (2006)
C. Mayer, T. Maier, Geophys. J. Int. **167**, 1188 (2006)
A. Namgaladze, M.M. Förster, R. Yurik, Ann. Geophys. **18**, 461 (2000)
T. Neubert, M. Mandea, G. Hulot, R.V. Frese, F. Primdahl, J.L. Jørgensen, E. Friis-Christensen, P. Stauning, N. Olsen, T. Risbo, Eos **82**(7), 81 (2001)
P.T. Newell, T. Sotirelis, K. Liou, C.-I. Meng, F.J. Rich, J. Geophys. Res. **112**(A1) (2007). doi:10.1029/2006JA012015
N. Olsen, M. Mandea, Nat. Geosci. **1**, 390 (2008)
N. Olsen, T.J. Sabaka, L. Tøffner-Clausen, Earth Planets Space **52**, 1175 (2000)
N. Olsen, F. Lowes, T.J. Sabaka, Earth Planets Space **57**, 1191 (2005)
N. Olsen, T. Sabaka, F. Lowes, Earth Planets Space **57**, 1141 (2005)
N. Olsen, H. Lühr, T.J. Sabaka, M. Mandea, M. Rother, L. Tøffner-Clausen, S. Choi, Geophys. J. Int. **166**, 67 (2006)
N. Olsen, M. Mandea, T.J. Sabaka, L. Tøffner-Clausen, Geophys. J. Int. **179**, 1477 (2009)
N. Olsen, M. Mandea, T.J. Sabaka, L. Tøffner-Clausen, Earth Planets Space **62**, 719 (2010)
N. Olsen, E. Friis-Christensen, R. Floberghagen, P. Alken, C.D. Beggan, A. Chulliat, E. Doornbos, J.T. da Encarnação, B. Hamilton, G. Hulot, J. van den IJssel, A. Kuvshinov, V. Lesur, H. Lühr, S. Macmillan, S. Maus, M. Noja, P.E.H. Olsen, J. Park, G. Plank, C. Püthe, J. Rauberg, P. Ritter, M. Rother, T.J. Sabaka, R. Schachtschneider, O. Sirol, C. Stolle, E. Thébault, A.W.P. Thomson, L. Tøffner-Clausen, J. Velímský, P. Vigneron, P.N. Visser, Earth Planets Space **65**, 1189 (2013)
N. Olsen, H. Lühr, C. Finlay, T.J. Sabaka, I. Michaelis, J. Rauberg, L. Tøffner-Clausen, Geophys. J. Int. **197**(2), 815 (2014)
N. Olsen, G. Hulot, V. Lesur, C.C. Finlay, C. Beggan, A. Chulliat, T.J. Sabaka, R. Floberghagen, E. Friis-Christensen, R. Haagmans, S. Kotsiaros, H. Luehr, L. Tøffner-Clausen, P. Vigneron, Geophys. Res. Lett. **42**, 1092 (2015)
N. Olsen, C.C. Finlay, S. Kotsiaros, L. Tøffner Clausen Earth Planets Space (2016). doi:10.1186/s4063-016-0488z
N. Olsen, E. Friis-Christensen, G. Hulot, M. Korte, A.V. Kuvshinov, V. Lesur, H. Lühr, S. Macmillan, M. Mandea, S. Maus, M. Purucker, C. Reigber, P. Ritter, M. Rother, T. Sabaka, P. Tarits, A. Thomson, Swarm—End-to-End mission performance simulator study, ESA contract No. 17263/03/NL/CB, DSRI Report 1/2004 (Danish Space Research Institute, Copenhagen)
R. Parker, *Geophysical Inverse Theory* (Princeton University Press, Princeton, 1994)
M. Purucker, K. Whaler, in *Treatise on Geophysics*, vol. 5, ed. by M. Kono (Elsevier, Amsterdam, 2007), pp. 195–235
C. Püthe, A. Kuvshinov, A. Khan, N. Olsen, Geophys. J. Int. **203**(3), 1864 (2015)
J.M. Quinn, R.J. Coleman, S. Macmillan, D.R. Barraclough, J. Geomagn. Geoelectr. **49**, 245 (1997)
A.D. Richmond, J. Geomagn. Geoelectr. **47**, 191 (1995)
A.D. Richmond, J.P. Thayer, Ionospheric electrodynamics: a tutorial, in *Magnetospheric Current Systems* (American Geophysical Union, Washington, 2000), pp. 131–146
H. Rishbeth, J. Inst. Electron. Radio Eng. **58**(6), 207 (1988)
M. Rother, V. Lesur, R. Schachtschneider, Earth Planets Space **65**, 1223 (2013)
C.T. Russell, R.L. McPherron, J. Geophys. Res. **78**, 92 (1973)
T.J. Sabaka, R.T. Baldwin, Modeling the Sq magnetic field from POGO and Magsat satellite and contemporaneous hourly observatory data: phase I (1993)
T.J. Sabaka, R.A. Langel, R.T. Baldwin, J.A. Conrad, J. Geomagn. Geoelectr. **49**, 157 (1997)
T.J. Sabaka, N. Olsen, R.A. Langel, A comprehensive model of the near-earth magnetic field: phase 3. NASA GSFC, Greenbelt, MD 20771 (2000)
T.J. Sabaka, N. Olsen, R.A. Langel, Geophys. J. Int. **151**, 32 (2002)

T.J. Sabaka, N. Olsen, M.E. Purucker, Geophys. J. Int. **159**, 521 (2004)
T.J. Sabaka, L. Tøffner-Clausen, N. Olsen, Earth Planets Space **65**, 1201 (2013)
T.J. Sabaka, N. Olsen, R. Tyler, A. Kuvshinov, Geophys. J. Int. **200**, 1596 (2015)
J.-J. Schott, E. Thébault, in *Geomagnetic Observations and Models*, ed. by M. Mandea, M. Korte Chap. IAGA Special Sopron Book Series, vol. 5 (Springer, Berlin, 2011), Chap. 9
L. Shure, R. Parker, G. Backus, Phys. Earth Planet. Inter. **28**, 215 (1982)
M. Sugiura, T. Kamei, Equatorial D_{st}-index 1957–1986. IAGA Bulletin No. 40 (1991)
E. Thébault, F. Vervelidou, V. Lesur, M. Hamoudi, Geophys. J. Int. **188**, 891 (2012)
E. Thébault, C.C. Finlay, P. Alken, C.D. Beggan, E. Canet, A. Chulliat, B. Langlais, V. Lesur, F.J. Lowes, C. Manoj et al., Earth Planets Space **67**(1), 112 (2015a). doi:10.1186/s40623-015-0273-4
E. Thébault, C.C. Finlay, C.D. Beggan, P. Alken, J. Aubert, O. Barrois, F. Bertrand, T. Bondar, A. Boness, L. Brocco et al., Earth Planets Space **67**(1), 79 (2015b). doi:10.1186/s40623-015-0228-9
E. Thébault, C.C. Finlay, H. Toh, Earth Planets Space **67**(1), 158 (2015c)
E. Thébault, V. Lesur, K. Kauristie, R. Shore, Space Sci. Rev. (2016a), submitted
E. Thébault, P. Vigneron, B. Langlais, G. Hulot, Earth Planets Space **68** (2016b)
A.W.P. Thomson, V. Lesur, Geophys. J. Int. **169**(3), 951 (2007)
A. Thomson, B. Hamilton, S. Macmillan, S. Reay, Geophys. J. Int. **181**, 250 (2010)
N. Tsyganenko, J. Geophys. Res. **105**, 27739 (2000)
N.A. Tsyganenko, J. Geophys. Res. **107**(A8), 12 (2002a)
N.A. Tsyganenko, J. Geophys. Res. **107**(A8), 10 (2002b)
V. Vasyliunas, in *Particles and Fields in the Magnetosphere*, ed. by B.M. McCormac (Springer, Netherlands, 1970), pp. 60–71
S. Vennerstrom, F. Christiansen, N. Olsen, T. Moretto, Geophys. Res. Lett. **34**, L16101 (2007). doi:10.1029/2007GL030175
D.R. Weimer, J. Geophys. Res. Space Phys. **110** (2005)
D. Weimer, Space Weather **11**, 107 (2013)
D.R. Weimer, C.R. Clauer, M.J. Engebretson, T.L. Hansen, H. Gleisner, I. Mann, K. Yumoto, J. Geophys. Res. Space Phys. **115**(A10) (2010). doi:10.1029/2010JA015540
P. Wessel, J. Becker, Geophys. J. Int. **174**, 21 (2008)
K. Whaler, R. Langel, Phys. Earth Planet. Inter. **48**, 303 (1996)
K. Whaler, M. Purucker, J. Geophys. Res. **110** (2005). doi:10.1029/2004JE002393
E.E. Woodfield, M. Dunlop, R. Holme, J. Davies, M. Hapgood, J. Geophys. Res. **112**, A06248 (2007). doi:10.1029/2006JA012217
Q.-H. Zhang, M. Dunlop, R. Holme, E. Woodfield, Ann. Geophys. **28**, 309 (2010)